atmosphere

MDPI

Article

Climatological Assessment of GHGs in Greece from over Two Decades of CAMS Atmospheric Composition Data (2003–2024)

Marios Mermigkas [1,*], Stergios Kartsios [1,2], Anna Kampouri [1], Jonilda Kushta [3] and Vassilis Amiridis [1]

[1] Institute for Astronomy, Astrophysics, Space Applications and Remote Sensing, National Observatory of Athens, 10560 Athens, Greece; skartsios@noa.gr (S.K.)
[2] Department of Meteorology and Climatology, School of Geology, Aristotle University of Thessaloniki, 54124 Thessaloniki, Greece
[3] Climate and Atmosphere Research Center, The Cyprus Institute, 2121 Nicosia, Cyprus
* Correspondence: mmermigk@noa.gr

Abstract

This study analyzes climatological trends and variability of the main greenhouse gases (GHGs)—carbon dioxide (CO_2), methane (CH_4), and carbon monoxide (CO)—over Greece using Copernicus Atmosphere Monitoring Service (CAMS) data (EAC4 and EGG4) alongside global emission inventories and satellite-derived fluxes. A statistically significant positive long-term trend was identified for both CO_2 and CH_4. CO_2 concentrations have been increased by approximately 2 ppm/year, reaching over 415 ppm in 2020 compared to 380 ppm in 2003, following the global trends of ground-based measurements in the northern hemisphere. CH_4 showed a rapid increase since 2007, linked to anthropogenic activities, although natural sources also contribute. In contrast, CO exhibits a negative trend of about 0.6 ppb/year, with significant seasonal variability due to both anthropogenic sources and wildfires. Notably, CO concentrations increased during wildfire episodes in 2021 and 2023, with enhanced CO concentrations over 100 $\pm$ 20 ppb, well above typical summer values of 80 $\pm$ 10 ppb. Both CO_2 and CH_4 exhibit positive seasonal anomalies relative to the 2003–2013 reference period. Analysis of short- and mid-term variability reveals that CO_2 fluctuates within $\pm$0.5%, with higher winter concentrations linked to anthropogenic emissions, while CH_4 variability reaches $\pm$2%, reflecting diverse urban, industrial, and agricultural sources. CO exhibits the highest variability ($\pm$10–50%) due to its shorter atmospheric lifetime and sensitivity to local emissions and wildfire events. Sectoral comparisons with the Greek National Inventory Report indicate a general decline in GHG emissions in Greece, although sector-specific differences persist. Seasonal patterns show elevated fossil CO_2 emissions during colder months, CH_4 emissions peaking in agricultural seasons, and CO peaks during summer wildfires. In general, CAMS GHG emission trends fall well within the National Inventory Report of Greece. These findings emphasize the importance of combining long-term trends with short- and mid-term variability to capture both anthropogenic and natural influences on GHGs, providing a more comprehensive understanding of emission dynamics in Greece, when global warming and climate change remain an inherently challenging issue during the last decades.

Keywords: CAMS; greenhouse gases; climatology; trend; CO_2; CO; CH_4; Greece; growth rate; emission fluxes

Academic Editors: László Haszpra and Yongming Han

Received: 12 February 2026
Revised: 7 April 2026
Accepted: 9 April 2026
Published: 13 April 2026

1. Introduction

1.1. Atmospheric Greenhouse Gases and Their Climate Impact

The continuous rise in atmospheric greenhouse gases (GHGs) remains one of the clearest and most concerning indicators of anthropogenic climate change, with major implications for the Earth's system, including radiative forcing, carbon cycle feedback, atmospheric chemistry, and regional climate impacts. Water vapor (H_2O), carbon dioxide (CO_2), methane (CH_4), and nitrous oxide (N_2O) are the primary greenhouse gases that trap heat near the Earth's surface. Their natural levels in the atmosphere are regulated by processes such as photosynthesis and respiration in the case of carbon dioxide or methane production by microorganisms in wetlands. However, human activities—particularly since the industrial revolution—have significantly increased the concentration of these gases, leading to an accelerated warming of the Earth's climate. Among these gases, CO_2 and CH_4 are the dominant long-lived GHGs, while carbon monoxide (CO) plays a key role as an indirect greenhouse gas (GHG) and tracer of biomass burning. CH_4, whose warming potential is about 28 times that of carbon dioxide over 100 years and roughly 80 times stronger over 20 years, has risen to an atmospheric concentration of 1923 parts per billion (ppb) as of 2023, driving GHG trends in the opposite direction of what is needed to maintain a habitable planet and limit global warming below even 2 °C [1]. Natural sources of methane in Greece primarily include the anaerobic decomposition of organic matter in wetlands, which accounts for a significant portion of global methane emissions. Other natural sources include the emissions from geological processes, such as seepage from natural gas deposits, and methane release from certain animal species in ecosystems like wetlands and forests. On the anthropogenic side, methane is predominantly emitted from agricultural practices (particularly rice cultivation, livestock, and manure management), fossil fuel extraction and use, and waste management activities like landfills. Approximately 40% of the CH_4 released into the atmosphere comes from natural sources such as wetlands and termites, while the remaining 60% originates from human activities including ruminant livestock, rice cultivation, fossil fuel extraction, landfills, and biomass burning [2]. The dominant atmospheric sink of methane is its oxidation by hydroxyl radicals (OH), particularly during summer when photochemical activity is strongest. This process contributes to the seasonal minimum observed in CH_4 concentrations. CO's relatively short atmospheric lifetime allows it to be transported over long distances, making it a useful marker for identifying distant sources of combustion, including wildfires and agricultural burning. CO, one of the most important atmospheric pollutants, is primarily produced by inefficient combustion, such as biomass burning [3], traffic, and industrial activity [4]. In addition to its role as a precursor for the formation of secondary pollutants such as ozone, CO modulates atmospheric chemistry by influencing the concentration of OH, which in turn affects the lifetime of CH_4 in the atmosphere. In the troposphere, CO reacts with OH in the reaction $CO + \cdot OH \rightarrow CO_2 + \cdot H$ [5,6], which indirectly affects the lifetime of CH_4 by reducing the availability of OH that would otherwise oxidize CH_4. Despite its short-lived nature, with a lifetime typically ranging from weeks to months, CO plays an indirect but significant role in climate forcing. Thus, by modulating the abundance of OH, CO helps control the atmospheric lifetime of CH_4 and facilitates tropospheric ozone formation, both of which are important components of climate forcing [7]. Consequently, CO provides a valuable diagnostic tool for understanding regional combustion activity and transport processes, complementing CO_2 and CH_4 observations in studies of atmospheric composition and climate change. In Greece, CO_2 emissions are predominantly linked to energy production, transportation, and industry, although the transition to renewable energy sources, such as wind and solar, has contributed to a decline in the carbon intensity of the energy sector over the past two decades [8]. However, challenges remain in sectors like transportation,

residential heating, and biomass burning, where fossil fuel consumption continues to be significant. CH_4 emissions in Greece, on the other hand, are heavily driven by agriculture, particularly livestock farming, as well as methane leaks from landfills and the oil and gas sectors. Given methane's potency as a greenhouse gas, reducing these emissions could provide immediate climate benefits and comply with the Paris Climate Agreement and the Global Methane Pledge. Greece, located at the interface of Mediterranean, continental, and marine climate regimes, exhibits a distinct regional signature in greenhouse gas variability due to its complex topography, strong coastal influences, urban–industrial activity, and seasonal biomass burning. CO_2 emissions are primarily associated with energy production, transportation, and industrial processes, whereas CH_4 mainly originates from agriculture and waste management, with additional natural contributions from wetlands. CO, a short-lived species, shows pronounced seasonal variability, with elevated levels during wildfire events and biomass burning, and is commonly used as a tracer of combustion processes. The interplay between these emission sources and dynamic meteorological conditions makes Greece a particularly suitable case study for investigating temporal variability in CO_2, CH_4, and CO, as well as for interpreting trends and anomalies and their implications for air quality management and climate mitigation.

1.2. Global Trends and Recent Research Findings

Globally, the burden of atmospheric greenhouse gases continues to rise at alarming rates. According to the World Meteorological Organization (WMO) Greenhouse Gas Bulletin No. 21 (https://wmo.int/sites/default/files/2025-10/GHG-21_en.pdf, accessed on 1 December 2025), the globally averaged surface mole fractions of CO_2 reached 423.9 ± 0.2 ppm, 1 942 ± 2 ppb for CH_4, and 338.0 ± 0.1 ppb for N_2O in 2024—all new record highs. The year to year increase in CO_2 (≈3.5 ppm from 2023 to 2024) was the largest ever observed, reflecting continued fossil fuel emissions, extensive wildfires, and possible weakening of land and ocean sinks during the 2023–2024 El Niño event (https://wmo.int/sites/default/files/2025-10/GHG-21_en.pdf, accessed on 1 December 2025). Meanwhile, for 2023, the WMO press release noted that CO_2 reached 420.0 ± 0.1 ppm (≈151% of the pre-industrial level) and CH_4 a record 1934 ± 2 ppb (≈266% of pre-industrial), with concerns about sink strength and carbon cycle feedback (https://public.wmo.int/news/media-centre/greenhouse-gas-concentrations-surge-again-new-record-2023, accessed on 1 December 2025).

According to NOAA's globally averaged marine surface data [9], methane has exhibited particularly strong and variable growth over the last decade. Following a plateau in the early 2000s, CH_4 concentrations began accelerating again around 2007, with an even steeper rise after 2020. Atmospheric methane concentrations have been increasing steadily since 2007 and, by 2024, were more than 2.5 times higher than pre-industrial levels [1]. According to the latest WMO bulletin [10], the globally averaged CH_4 concentration calculated from in situ observations reached a new high of 1942 ± 2 ppb in 2024, an increase of 8 ppb with respect to the previous year [2]. The growth rate shows an increasing tendency, although it has not yet reached a stable level [9].

Remote sensing of CO_2 and CH_4 with both ground-based measurements and satellite observations reveal an increased trend in these GHGs, captured by recent studies. One study [11] showed a positive consistent CO_2 growth rate of 3.2 ppm/year in Paris, France, for three different sites, with a discernible seasonal cycle, using FTIR spectrometers and in situ data. Also, measurements of column averaged dry air mole fractions of CO_2, CH_4, and CO performed in Thessaloniki [12] and other cities in the northern hemisphere using the portable ground-based EM27/SUN, part of the Collaborative Carbon Column Observing Network (COCCON) [13–15], showed a growth rate of CO_2 of over 2 ppm/year and also

a positive trend in CH_4. In addition, observations from the TROPOspheric Monitoring Instrument (TROPOMI) onboard Sentinel-5P revealed increased CH_4 observations around Thessaloniki, Greece [16]. In addition, one study [17] confirms the long-term positive trend of GHGs in Greek regions, using both ground-based measurements and satellite observations.

Carbon monoxide presents a contrasting picture. Long-term global analyses [18] indicate that CO has been declining since the early 2000s due to cleaner combustion technologies, improved vehicle emission controls, and reduced biomass burning in certain regions. However, the overall decline in certain atmospheric constituents has slowed in recent years, and regional increases have been observed, particularly in association with large wildfires, urban pollution, or drought-driven biomass burning in the Mediterranean region and the tropics. A recent study [19] found that increased CO concentrations are driven by wildfire episodes, captured in Thessaloniki by a portable EM27/SUN FTIR spectrometer, leading to an unprecedented increase in concentrations of CO by over 130% compared to the typical averaged mean values during summer time in Greece. Thus, CO remains an important diagnostic for short-term atmospheric composition variability and as an indicator of wildfire-driven emission anomalies. Although overall anthropogenic CO emissions in Europe have declined over recent decades due to technological improvements and regulatory measures, local pollution levels remain significant, particularly during temperature inversion events or in areas with increased heating-related combustion. The role of these emissions in atmospheric pollution becomes even more critical when combined with natural sources, such as wildfires, which appear to have driven the seasonal variability of carbon monoxide in Greece (as well as in other Mediterranean countries) in recent years.

To supplement ground-based and satellite observations, the Copernicus Atmospheric Monitoring Service (CAMS) provides a high-quality and accurate tool for atmospheric observations, filling the gap of in situ measurements. In a recent study, CAMS revealed a positive trend of both CO_2 and CH_4 in three countries in the northern hemisphere, Greece, Italy, and France [20]. It is worth mentioning that a study [21] reports that changes in the assimilated satellite data have a clear impact on the evolution of the global annual mean values of CO_2 and CH_4. In summary, while CO_2 and CH_4 continue to increase globally with record-high growth rates, CO's variability reflects shorter-term processes and regional emission changes.

1.3. Objectives and Scope of This Study

This study presents a comprehensive climatological analysis of CO_2, CH_4, and CO over Greece using two decades of CAMS reanalysis data, with several key objectives: quantifying long-term trends and seasonal cycles of these gases through the CAMS-EGG4 and EAC4 datasets; investigating mid-term and short-term variability to capture intra-seasonal and diurnal fluctuations; identifying anomalies and extreme years (e.g., 2016, 2020, 2021, 2023, and 2024) in relation to major climate events, such as heatwaves, wildfires, and El Niño-related variability; and comparing regional patterns across Greece to assess spatial heterogeneity in atmospheric behavior.

This study aims to provide new insights into the behavior of key greenhouse gases in the Mediterranean region, with a focus on the influence of local and regional emission sources and meteorological conditions on atmospheric composition. It further evaluates the implications of these trends for climate change and air quality mitigation. The results contribute to a better understanding of the interaction between large-scale climatic drivers and local emission processes in shaping atmospheric composition over southeastern Europe. The Mediterranean region, characterized by complex topography, strong land–sea contrasts, diverse urban and industrial emissions, and frequent biomass burning events, provides an

ideal natural laboratory for investigating the interplay between long-term climatological trends and regional-scale processes. Overall, this work supports ongoing efforts to improve greenhouse gas monitoring and to better understand regional feedback mechanisms in the context of climate change.

2. Data and Methods

2.1. Overview of Datasets

This study employs two Copernicus Atmosphere Monitoring Service (CAMS) reanalysis products—CAMS-EAC4 (https://ads.atmosphere.copernicus.eu/datasets/cams-global-reanalysis-eac4?tab=overview, accessed on 1 December 2025) and CAMS-EGG4 (https://ads.atmosphere.copernicus.eu/datasets/cams-global-ghg-reanalysis-egg4?tab=overview, accessed on 1 December 2025)—to analyze the climatological and inter-annual variability of atmospheric CO_2, CH_4, and CO over Greece for the period of 2003–2024. These reanalysis datasets combine advanced atmospheric chemistry models with extensive satellite and in situ observations through four-dimensional variational (4D-Var) data assimilation, providing a spatially and temporally consistent record of atmospheric composition, while they are based on data assimilation systems that combine model forecasts with a wide range of satellite and in situ observations to provide globally consistent, high-resolution fields of atmospheric composition over decades [22].

1. CAMS-EAC4 (CH_4 and CO):

The CAMS Reanalysis of Atmospheric Composition, version 4 (EAC4), provides global fields of reactive gases, greenhouse gases, and aerosols [22]. It is based on the ECMWF Integrated Forecasting System (IFS) coupled with the MOZART-5 chemistry scheme. EAC4 assimilates satellite retrievals of CH_4 and CO (from instruments such as MOPITT, IASI, and AIRS), along with in situ measurements. The data are available at a horizontal resolution of $0.75^\circ \times 0.75^\circ$ on 60 vertical levels up to 0.1 hPa and at a 3-h temporal resolution. For this study, total columns of CH_4 and CO were extracted and spatially averaged over the Greek domain (approximately 34–42° N, 19–28° E). The resulting time series were used to analyze long-term trends, seasonal cycles, and variability.

2. CAMS-EGG4 (CO_2):

For CO_2, we used the CAMS Greenhouse Gas Reanalysis (EGG4), which extends the IFS framework with an optimized representation of the global carbon cycle and assimilation of satellite retrievals from GOSAT, OCO-2, and in situ flask measurements [21]. The dataset provides 3-h global fields of CO_2 mole fractions at the same spatial resolution ($0.75^\circ \times 0.75^\circ$). Reanalysis uses an assimilation system that detects observation biases, filters out poor-quality data, and fills gaps where measurements are sparse or nonexistent. The EGG4 CO_2 data were extracted over the same Greek domain to ensure spatial consistency with the EAC4 dataset. However, the EGG4 dataset currently extends only to 2020. Consequently, the CO_2 analysis in this study covers the period of 2003–2020.

Additionally, CAMS global emission inventories (https://ads.atmosphere.copernicus.eu/datasets/cams-global-emission-inventories?tab=overview, accessed on 1 December 2025) and CAMS global inversion-optimized greenhouse gas fluxes (https://ads.atmosphere.copernicus.eu/datasets/cams-global-greenhouse-gas-inversion?tab=overview, accessed on 1 December 2025) of CO_2 CO, and CH_4 are presented to gain a better understanding of how GHG emissions fluctuate over the years. The global emission inventory dataset contains gridded distributions of global anthropogenic and natural emissions. In this work, we use anthropogenic emissions with a spatial horizontal resolution of $0.1^\circ \times 0.1^\circ$, which are separated in specific activity sectors (e.g., power generation, road traffic, industry, agricultural, livestock, fugitives, waste, etc.). CAMS compiles inventories

of emission data that serve as input to its own forecast models but which can also be used by other atmospheric chemical transport models [23]. The CAMS global inversion-optimized greenhouse gas fluxes dataset contains net fluxes at the surface for carbon dioxide [24], methane [25], and nitrous oxide [26].

2.2. Methodology

To investigate sub-seasonal diurnal variability of greenhouse gases (GHGs), observational data using three complementary approaches were analyzed. Each one captures variability at different temporal scales, and they were performed separately for each meteorological season: winter (December–February), spring (March–May), summer (June–August), and autumn (September–November). Below, we present the main idea behind each case.

1. Rolling two-week window (short-term variations/dynamic climatology):

To capture continuous sub-seasonal variability, a rolling two-week window centered on each measurement (±7 days) was applied. For each timestamp, GHG measurements at the same hour of the day within the rolling window were averaged to define the reference value. Relative diurnal enhancements or sinks were expressed as the percentage deviation from the time-varying reference mean. Unlike fixed biweekly bins, the rolling window approach is more sensitive to short-term variability, enabling detection of transient emission events, rapid changes in atmospheric mixing, and gradual transitions between high- and low-concentration phases, while still filtering out long-term seasonal trends.

2. Biweekly fixed-bin climatology (mid-term variations):

To investigate the diurnal variability of GHGs on a sub-seasonal scale, we computed a biweekly 3-h climatology for each season. For each season, data were first filtered to include only the relevant months, and the seasonal time series was divided into consecutive two-week intervals to capture sub-seasonal variability while retaining sufficient temporal resolution. Within each two-week period, hourly GHG concentrations were grouped into three-hour bins to construct a diurnal cycle. For each biweekly, three-hour bin, the mean GHG concentration was calculated, serving as a reference climatological value for that period and hour. Relative diurnal enhancements and depletions were quantified as the percentage deviation of each measurement from the corresponding biweekly mean for each three-hour interval. This approach captures mid-term variability by smoothing short-term fluctuations while highlighting persistent patterns of greenhouse gas (GHG) enhancements and sinks within each season.

3. Long-term detrended 3-h mean diurnal variability:

In this case study, the long-term trend was first removed from the observational record, and the detrended data were classified by season and aggregated to a 3-h temporal resolution. Seasonal climatological diurnal cycles were then constructed from a multi-year reference period, and diurnal anomalies (ΔCO_2, ΔCO, ΔCH_4) were obtained by subtracting these seasonal baselines from the detrended observations. This procedure isolates enhancements and sinks—ranging from intra-day to synoptic timescales—by removing the seasonal diurnal pattern, thereby capturing both local sub-daily fluctuations and broader spatial dynamics. This provides insight into the interplay of emissions, atmospheric transport, and boundary layer processes. When computing seasonal three-hour climatologies from the detrended greenhouse gas (GHG) time series, extended fire events and other extreme episodes were excluded from the averages. This ensures that the resulting diurnal enhancements and sinks represent typical atmospheric variability, minimizing the influence of episodic or anomalous emissions on seasonal patterns.

Together, these three complementary approaches provide a robust characterization of GHG variability across multiple temporal scales. The fixed biweekly bins emphasize mid-term, sub-seasonal patterns; the rolling two-week window captures short-term, transient fluctuations; and the detrended hourly analysis isolates persistent diurnal signals by removing long-term trends and extreme events. To that end, by combining these methods, we ensure that both typical atmospheric variability and episodic anomalies are appropriately accounted for, enabling a comprehensive assessment of the temporal dynamics of CO_2, CO, and CH_4.

Furthermore, to capture long-term trends of GHGs for each year separately, relative to a long-term reference period (2003–2013), the climatological monthly mean for each GHG over the reference years was calculated. Monthly means for each year of interest were then calculated and subtracted from the corresponding climatological values to obtain the anomalies, which were further expressed as percentage deviations relative to the reference period. Spatial distributions of the anomalies were visualized over Greece using gridded observational data, with each month plotted separately to highlight seasonal and sub-seasonal variations. Also, the same methodology was applied to calculate seasonal anomalies over Greece relative to the same reference period.

3. Results

In this section, the long-term time series of GHGs are presented and analyzed, together with their seasonal cycles. In addition, we examine the anomalies of each gas (monthly and seasonal averaged) relative to the reference period of 2003–2013 over Greece. As a complementary way to visualize and further explore the data, heatmaps of monthly averaged total column abundances of GHGs are also presented. Finally, the short/mid-term variations (enhancements/sinks) of each gas are presented and analyzed to estimate possible emission sources, while long-term de-trended time series of Δ-gases are split into three sector bins (northern Greece, central Greece, and southern Greece) and compared to capture the highest variability over the years across different geographical regions. CAMS emission fluxes of CO_2 and CH_4 are also presented according to various sectors of interest in Greece, while CAMS emission rate inventories are shown in both spatial and temporal resolutions for CO_2 and CH_4, relative to specific emission sectors. In addition, we compare our findings of the emissions of CO_2, CH_4, and CO with both the Greek national report and the Emissions Database for Global Atmospheric Research (EDGAR) report, while the figures from CAMS inventories are shown in the Supplementary Materials (Figures S15–S23).

3.1. Long-Term Trends and Anomalies

3.1.1. Carbon Dioxide (CO_2)

Figure 1 shows the long-term daily mean time series of CAMS CO_2 product since 2003 along with corresponding monthly and annually means. We observe a constant positive trend of approximately 2 ppm per year and a strong seasonal cycle, which is that of a typical mid-latitude country in the northern hemisphere. Both anthropogenic emission sources and natural sinks drive this seasonality across years. Fossil fuel combustion, transport, heating, biomass burning, and industrial activities are the most important CO_2 emission sources in Greece. They occur mostly during winter and spring, while CO_2 emissions from fire episodes during summer account for a very small CO_2 enhancement in its concentrations. Sinks originate mainly from the terrestrial vegetation that binds CO_2 during the process of photosynthesis. The amplitude of the seasonal cycle in CO_2 is larger in the northern hemisphere than in the southern hemisphere, as northern hemispheric continents are the areas containing the majority of land plants covering the Earth's surface and the seasonal changes in temperature result in large differences in plant photosynthesis from summer

to winter. Photosynthesis results in decreased CO_2 in the local growing season, whereas photosynthesis gradually ceases and CO_2 builds up in autumn and winter [27]. Maximum CO_2 concentrations are found during late spring, reflecting the effect of anthropogenic sources, primarily driven by continued fossil fuel combustion from industrial activities and transportation, which remain significant as heating demand declines but energy use for production and mobility persists. Minimum CO_2 values are found during mid to late summer. The positive trend of CO_2 can be also identified by the heatmap in Figure 2, showing monthly averaged concentrations from 2003 to 2020. In 2020, CAMS reanalysis data depict a tremendous increase since 2003 with over 415 ppm, while CO_2 concentrations in 2003 did not exceed 380 ppm in Greece. The amplitude of the seasonal cycle for 2019–2020 is approximately 5 ppm and much more variable compared to the mean seasonal amplitude of the long-term period of 2003–2018, as shown in Figure 3. We observe a sharp decrease during 2019–2020 in the early spring seasonal mean, probably due to COVID-19 lockdown restrictions, which resulted in less GHG emissions during that period. The COVID-19 lockdown in Greece was implemented in multiple phases, beginning in March 2020 with nationwide restrictions on movement, closure of non-essential businesses, schools, and universities, and limitations on domestic and international travel. These measures, which lasted until late May 2020 with gradual easing, led to a substantial reduction in transportation, industrial activity, and overall energy demand, particularly in urban areas. The lockdown thus represents a short-term, national-scale intervention that temporarily lowered anthropogenic CO_2 emissions during 2020.

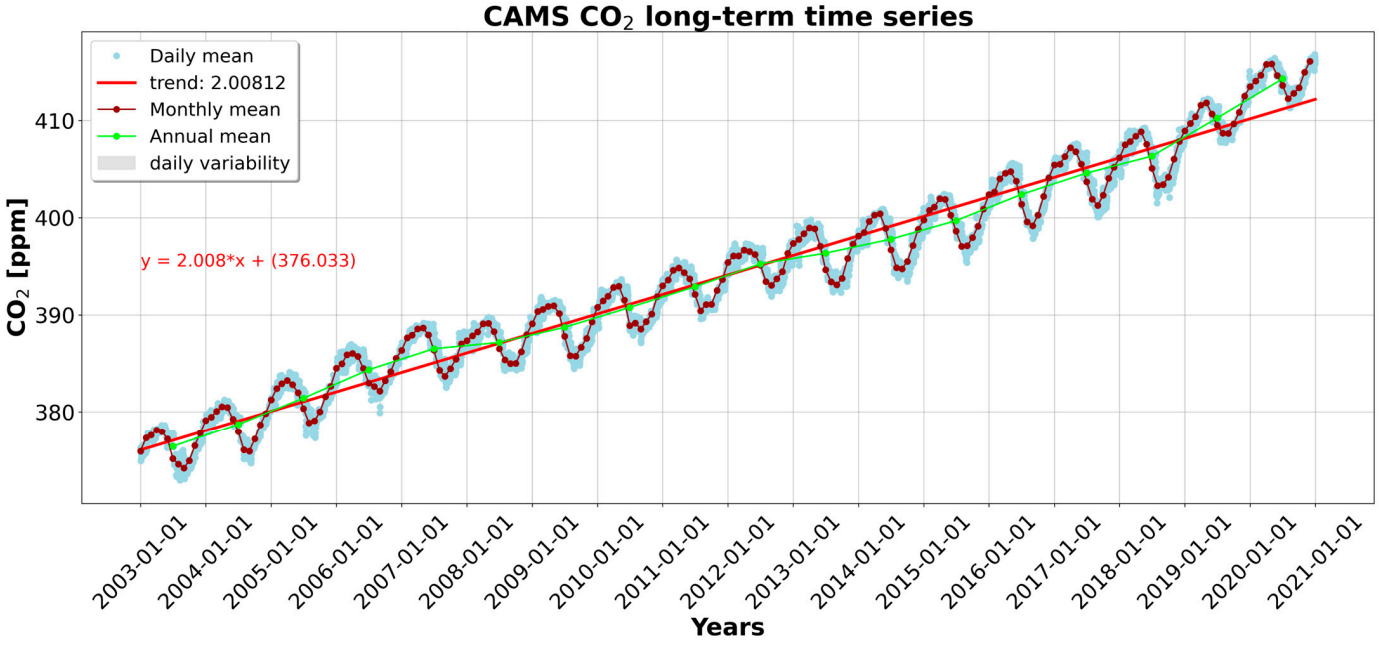

Figure 1. Long-term time series of total column concentrations of CO_2 over Greece covering the period of 2003–2020. The red line shows the trend, while dark red and blue dots represent the monthly mean and daily mean concentrations, respectively.

Additionally, we calculated the annual growth rate of CO_2 concentrations over Greece after removing the seasonal cycle in order to eliminate the strong effect of seasonal variations, consistent with [28]. A consistently high growth rate is observed across all years, ranging from 2 to 3 ppm yr^{-1}, while 2020 shows the largest increase, with CO_2 concentrations rising by over 4.5 ppm compared to the previous year.

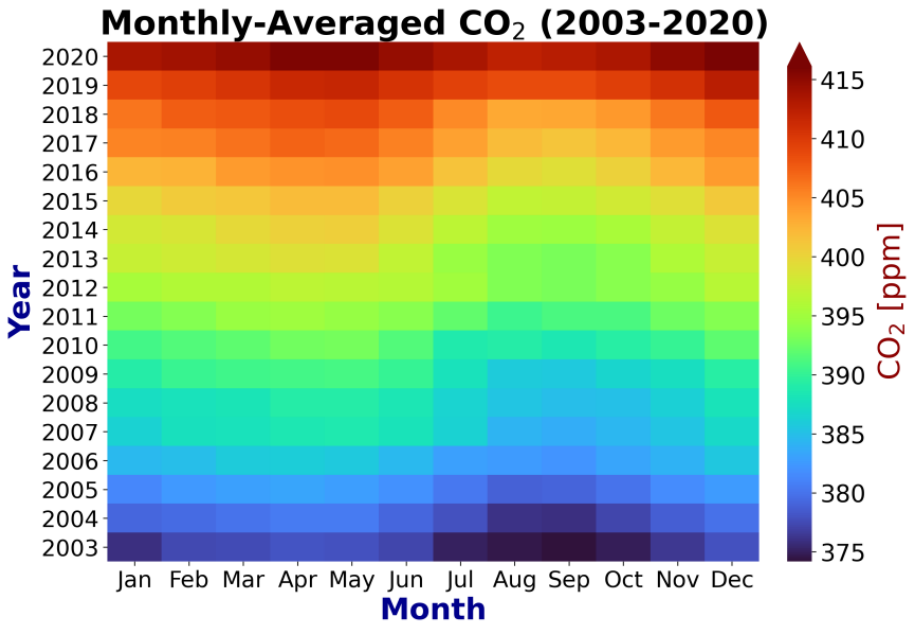

Figure 2. Monthly averaged heatmap of CO_2 over Greece per year.

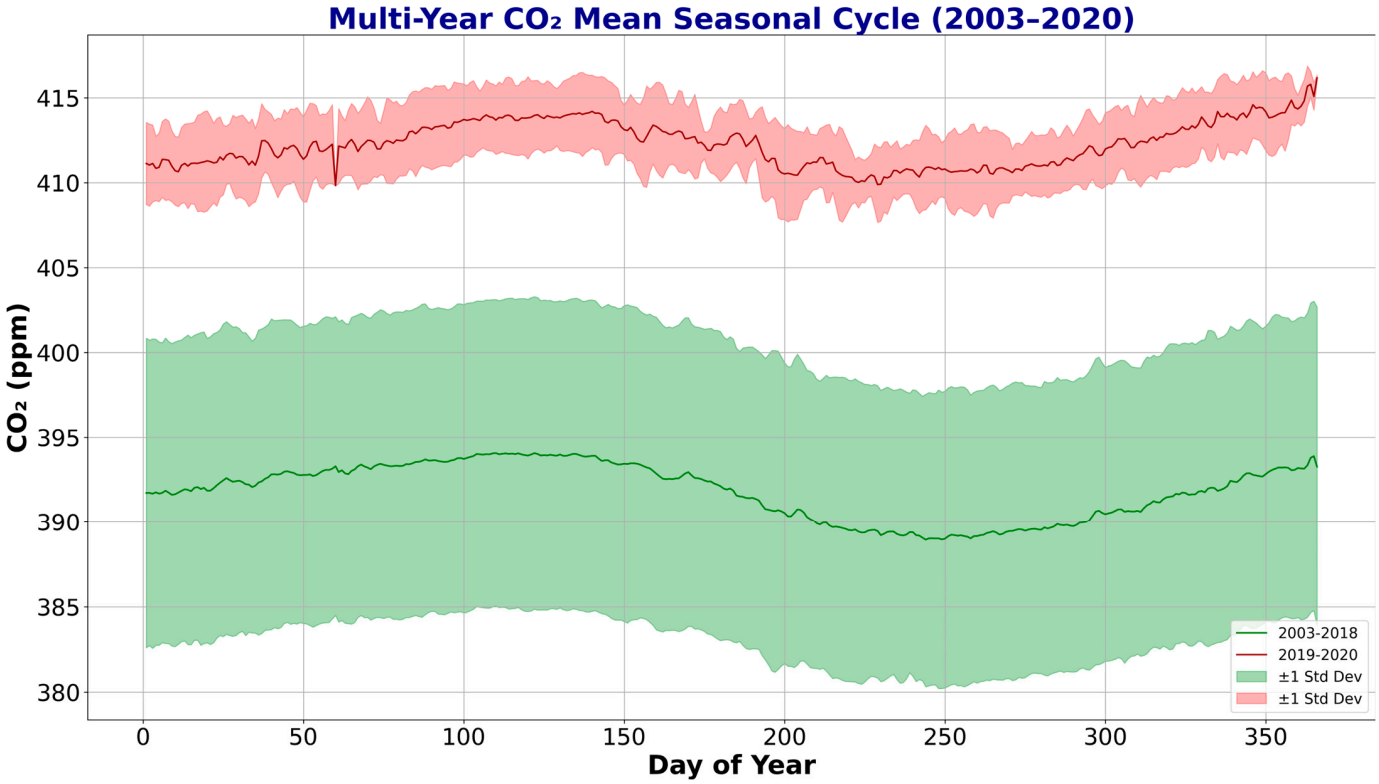

Figure 3. Seasonal cycle of CO_2 daily mean concentrations over Greece. The red solid line and light red shadow represent the daily mean concentrations between 2019 and 2020, while the green ones cover the longer period between 2003 and 2018.

Relative anomalies were derived as percentage deviations from the reference period according to the following formula:

$$\Delta CO_2\ [\%] = \left(\left(CO_{2year} - CO_{2climatology} \right) / \left(CO_{2climatology} \right) \right) * 100 \quad (1)$$

Figures 4 and 5 depict the monthly mean and seasonal mean anomalies of CO_2 relative to the reference period of 2003–2013. Regarding the monthly mean CO_2 anomalies, we see a clear upward trend in CO_2 concentrations, which peak in 2020, exceeding 20 ppm compared to the reference period. During winter and autumn of 2020, the highest seasonal mean CO_2 anomalies were observed (Figure 5), increasing by approximately 7–8 ppm. In comparison, the corresponding anomalies in 2019 ranged between 6 and 7 ppm. During spring and summer, CO_2 anomalies in 2020 were also elevated, rising by 6.5–7.5 ppm, whereas in 2019 they were lower at approximately 5 to 6 ppm.

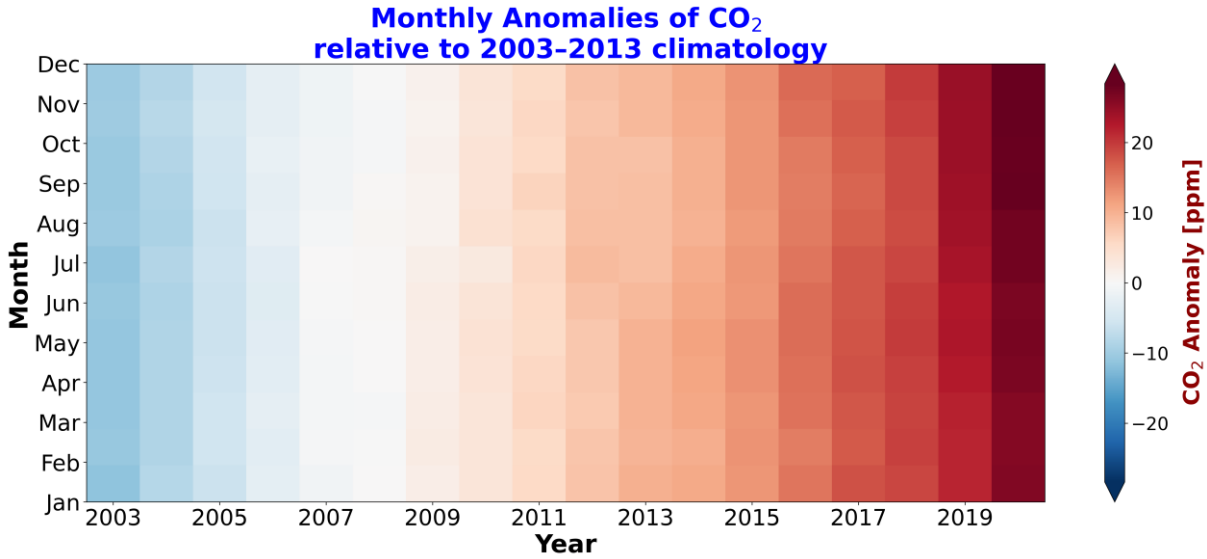

Figure 4. CO_2 anomalies over Greece relative to the reference period, 2003–2013.

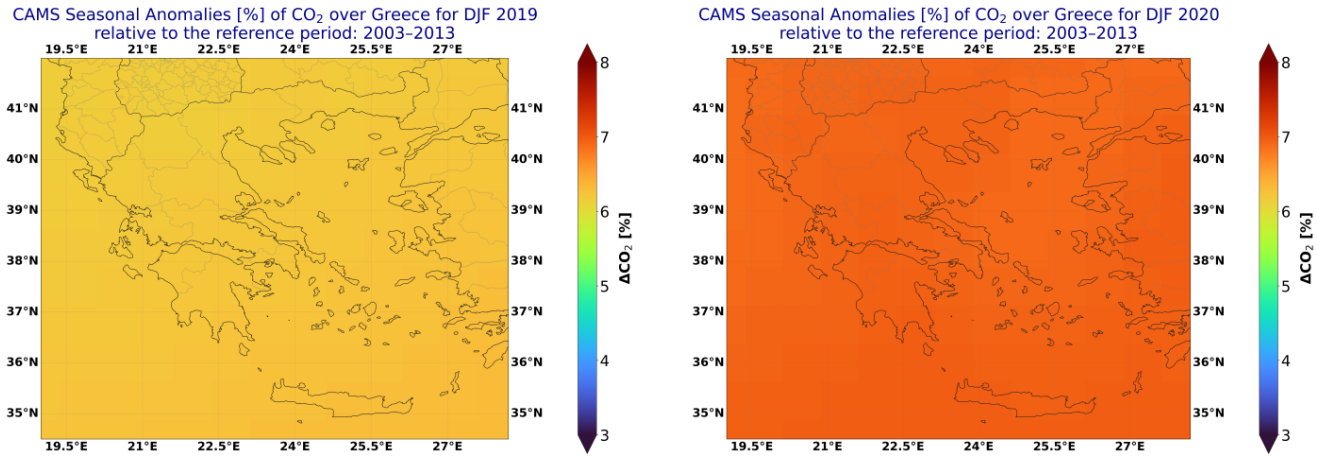

(**a**)

Figure 5. *Cont.*

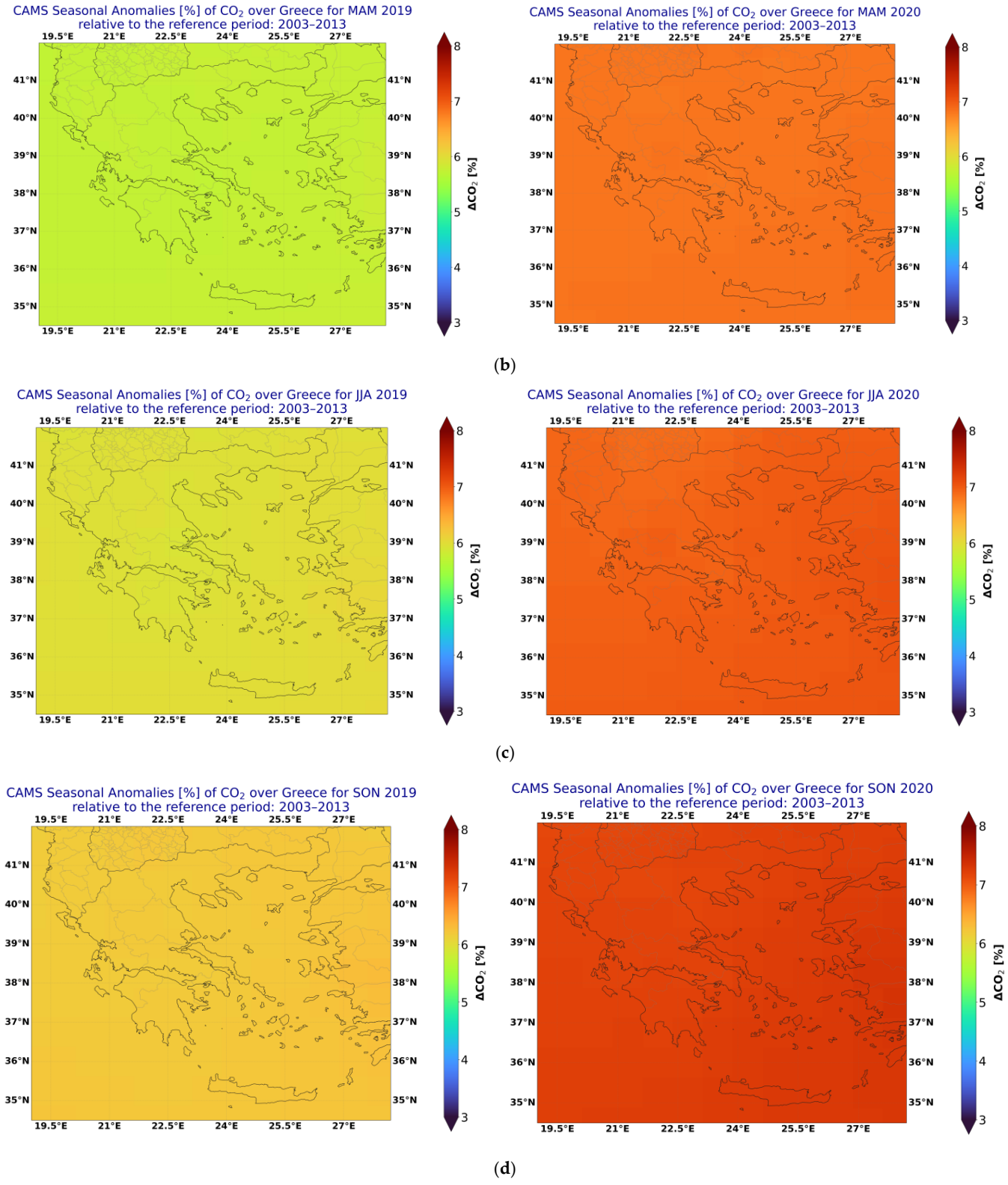

Figure 5. CAMS seasonal mean CO_2 anomalies over Greece for 2019 and 2020, relative to the reference period, for (**a**) DJF, (**b**) MAM, (**c**) JJA, and (**d**) SON.

3.1.2. Methane (CH_4)

Figure 6 presents the daily mean time series of CH_4 over Greece, together with the corresponding monthly and annual mean concentrations expressed in molecules/cm^2. A clear positive long-term trend is observed, although the annual growth rate appears

lower during the period of 2017–2022. The spatial and temporal distribution of methane emissions is influenced by factors such as temperature, seasonal agricultural cycles, and industrial activities. One of the major sinks for methane in the atmosphere is its reaction with hydroxyl radicals (OH), particularly during warmer months when OH concentrations are higher due to increased temperature (Figure 7). This reaction represents the dominant removal mechanism, although increasing methane levels can reduce OH concentrations, potentially leading to longer methane lifetimes in the atmosphere. The seasonal cycle of methane is driven by both emission sources (anthropogenic and natural) and sinks, yet it is more variable compared to CO_2, indicating the influence of multiple and diverse emission sources (Figure 8). Maximum concentrations are observed from early autumn to mid-winter, reflecting the combined influence of anthropogenic emissions and reduced photochemical removal. Minimum values are observed during summer as a result of enhanced oxidation by OH. Methane emissions originate from both natural and anthropogenic sources, including wetlands, agriculture (livestock and manure management), fossil fuel extraction, and waste management activities. The seasonal distribution of these sources, together with atmospheric chemistry, contributes to the observed variability.

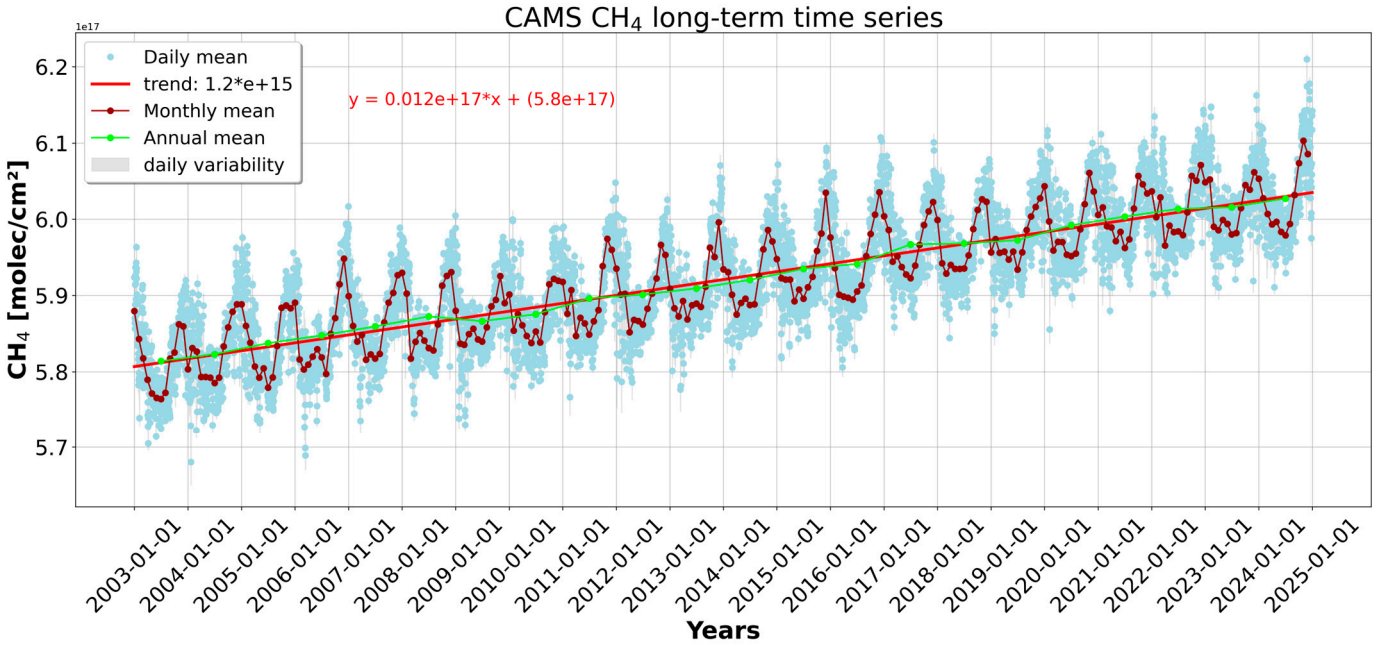

Figure 6. Long-term time series of total column concentrations of CH_4 over Greece covering the period of 2003–2004. The red line shows the trend, while dark red and blue dots represent the monthly mean and daily mean concentrations, respectively.

A discernible high growth rate is observed for all years, with values ranging from 1.8×10^{15} to 3.2×10^{15} molecules/cm^2/year.

Relative anomalies of CH_4 were derived as percentage deviations from the reference period, according to the following formula, as in the previous case of CO_2:

$$\Delta CH_4\ [\%]\ = \left(\left(CH_{4_{year}} - CH_{4_{climatology}} \right) / \left(CH_{4_{climatology}} \right) \right) * 100 \quad (2)$$

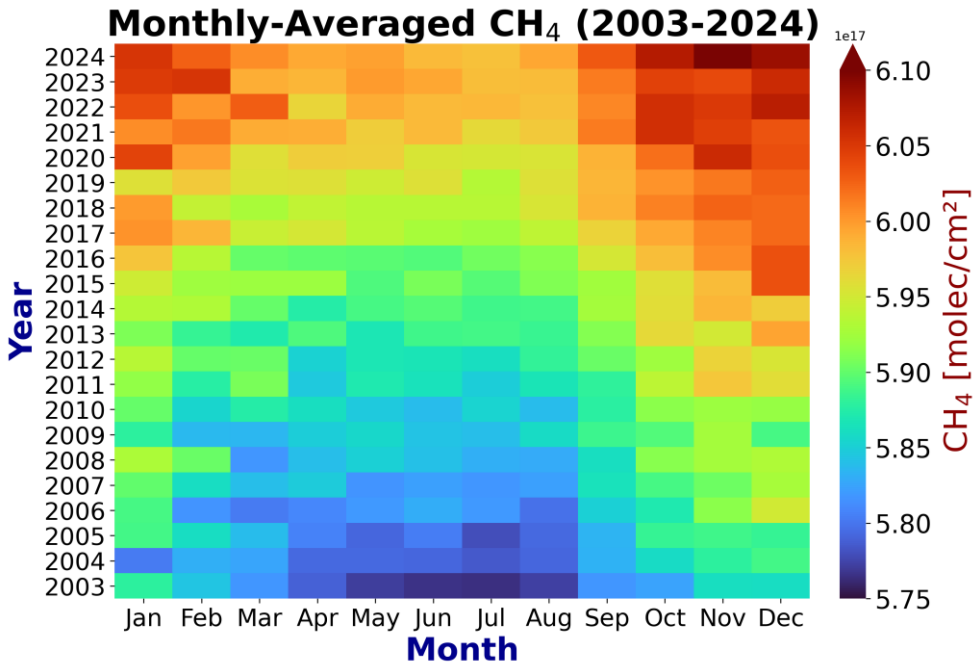

Figure 7. Monthly averaged heatmap of CH_4 over Greece per year.

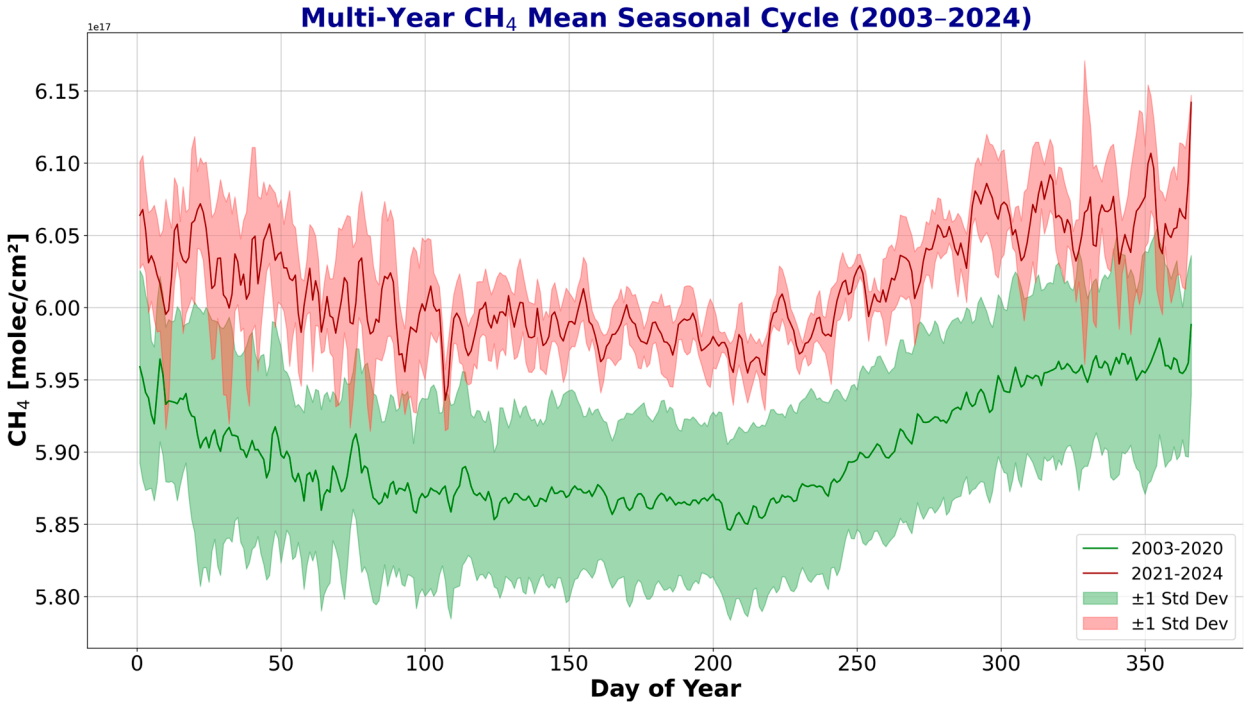

Figure 8. Seasonal cycle of CH_4 daily mean concentrations over Greece. The red solid line and light red shadow represent the daily mean concentrations between 2021 and 2024, while the green ones cover the longer period between 2003 and 2020.

Figures 9 and 10 depict the monthly mean and seasonal mean anomalies of CH_4 relative to the reference period of 2003–2013. Regarding the monthly mean CH_4 anomalies, we observe a clear upward trend in CH_4 concentrations, which peak during 2021–2024, exceeding 1.5×10^{16} molecules/cm^2 compared to the reference period. It is worth saying that CH_4 monthly anomalies show much more variability than CO_2 anomalies (Figure 4). In comparison, the corresponding anomalies in 2015 ranged between 6 and 7 ppm. During spring and summer, CO_2 anomalies in 2020 were also elevated, rising by 6.5–7.5 ppm,

whereas in 2019 they were lower at roughly 5–6 ppm. When comparing the seasonal CH_4 anomalies between 2015 and 2024, all seasons exhibit a positive trend, while the most significant increase was found during winter and autumn periods. In particular, winter 2024 shows an over 3% increase in methane concentrations, while spring and summer anomalies range from 2.25% to 2.75%. Notably, west of Thessaloniki, in northern Greece, a pronounced increase in CH_4 levels was found during summer (Figure 10c) and autumn periods (Figure 10d). This area is known for its persistent agricultural methane sources, which likely contribute to the observed rise in CH_4 concentrations, particularly during the growing seasons. In one study [29], observations from Sentinel-5 Precursor (S-5P) showed increased CH_4 concentrations in this particular area, with CH_4 emissions mainly originating from agriculture, farms, solid waste disposal in Thessaloniki, rice fields around Chalastra, or wastewater treatment. While CH_4 concentrations in Greece are influenced by the wildfire season, their contribution to the overall increase is relatively smaller compared to CO, as detailed in Section 3.1.3.

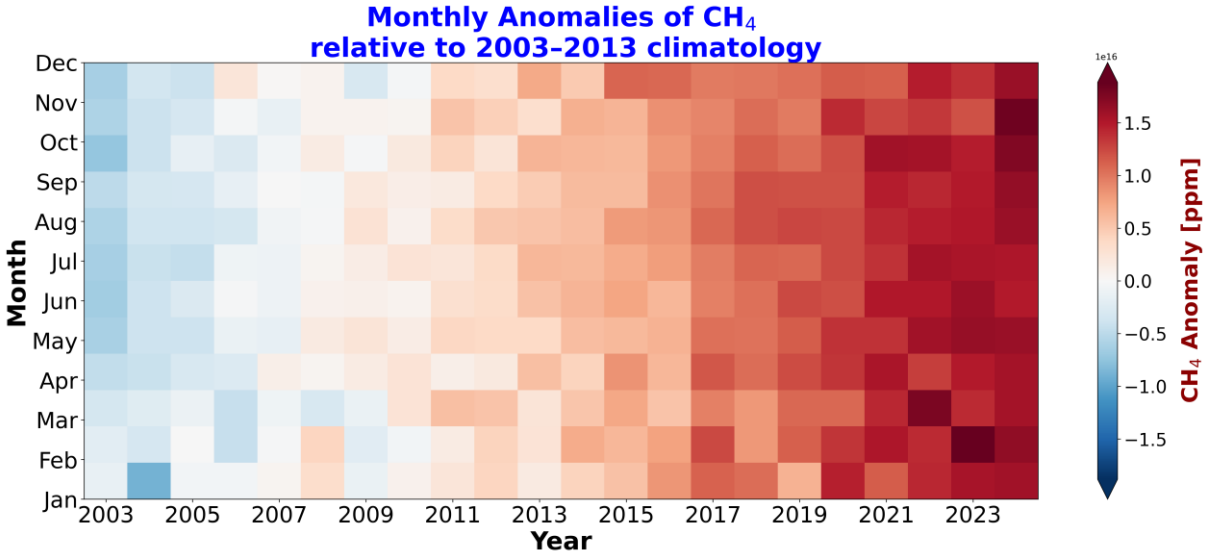

Figure 9. CH_4 anomalies over Greece relative to the reference period, 2003–2013.

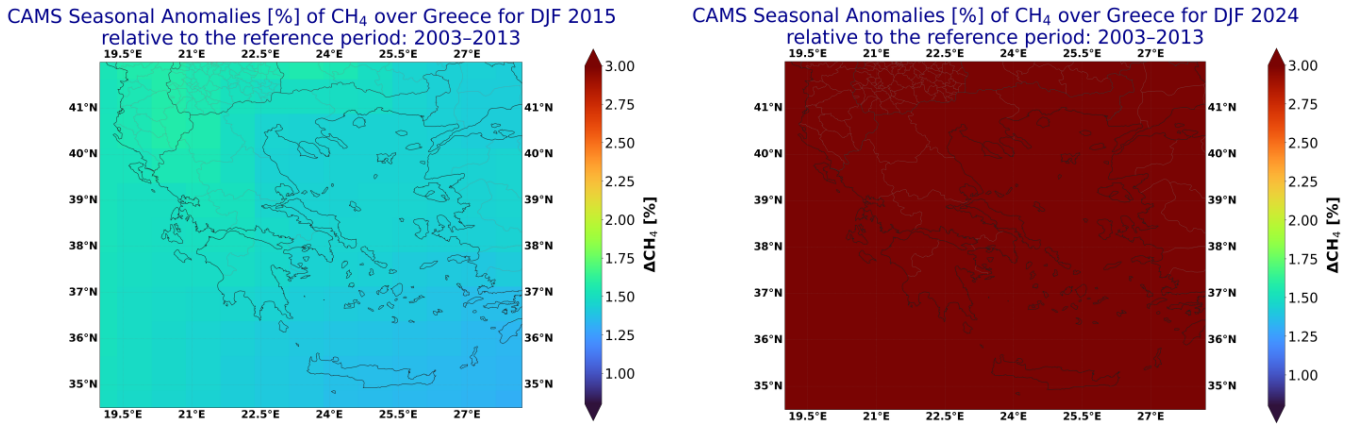

(**a**)

Figure 10. *Cont.*

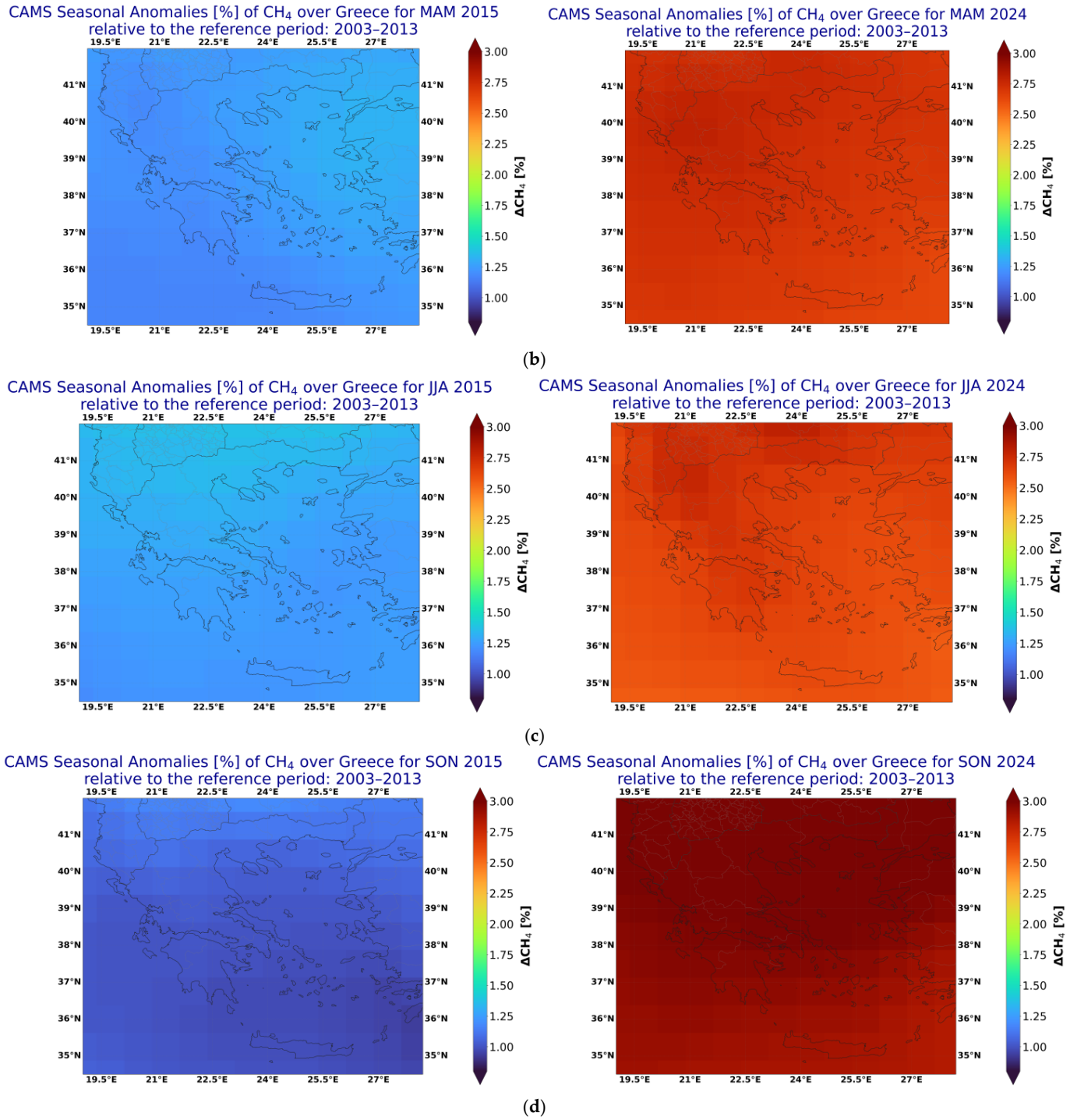

Figure 10. CAMS seasonal mean CH_4 anomalies over Greece for 2024 compared to 2015 for (**a**) DJF, (**b**) MAM, (**c**) JJA, and (**d**) SON.

3.1.3. Carbon Monoxide (CO)

Figure 11 presents the long-term trend of carbon monoxide (CO) concentrations in Greece for the period of 2003–2024. A pronounced decreasing trend is observed, reflecting the reduction of anthropogenic emissions associated with incomplete combustion of fossil fuels. Major sources include transportation, industrial activity, power generation, and biomass burning for residential heating or agricultural purposes. The dominant sink of CO is oxidation with OH [5]. Because CO's chemical reaction with OH is generally the major sink for OH in mid-latitude locations, the concentration and distribution of OH in

the atmosphere are often determined by CO [30]. Lower OH concentrations tend to reduce the rate of CO removal, so the inter-annual variability of OH perturbs long-term trends of CO levels [30]. We observe a negative trend of around 0.6 ppb/year and an autumn minimum and winter–spring maximum due to the influence of anthropogenic sources like incomplete combustion of fossil fuels as a consequence of traffic or heating, which constitute the primary source of XCO in the urban and densely populated cities of Greece, like Athens, Patra, Thessaloniki, and Heraklion. In recent years, wildfires in Greece have become more frequent and intense, largely due to climate change. The 2021 fire episodes in Athens and North Evia significantly elevated CO concentrations during the summer, while the 2023 fires in Alexandroupoli had a devastating impact [31], spreading across the western, southern, and southwestern regions of the country. The summer of 2024 was also characterized by severe wildfire activity, particularly in Athens, the Peloponnese, and other regions. Daily mean values shown in Figure 11 indicate CO concentrations exceeding 100 ppb, well above the typical summer average of 80 ppb. Figures 12 and 13 present the monthly averaged heatmap of CO over Greece per year and the seasonal cycle of CO daily mean concentrations over Greece, respectively. Although the seasonal mean values during 2021–2024 are less pronounced than in 2003–2020, substantially larger variability is observed in summer, reflecting the influence of fire episodes on CO concentrations.

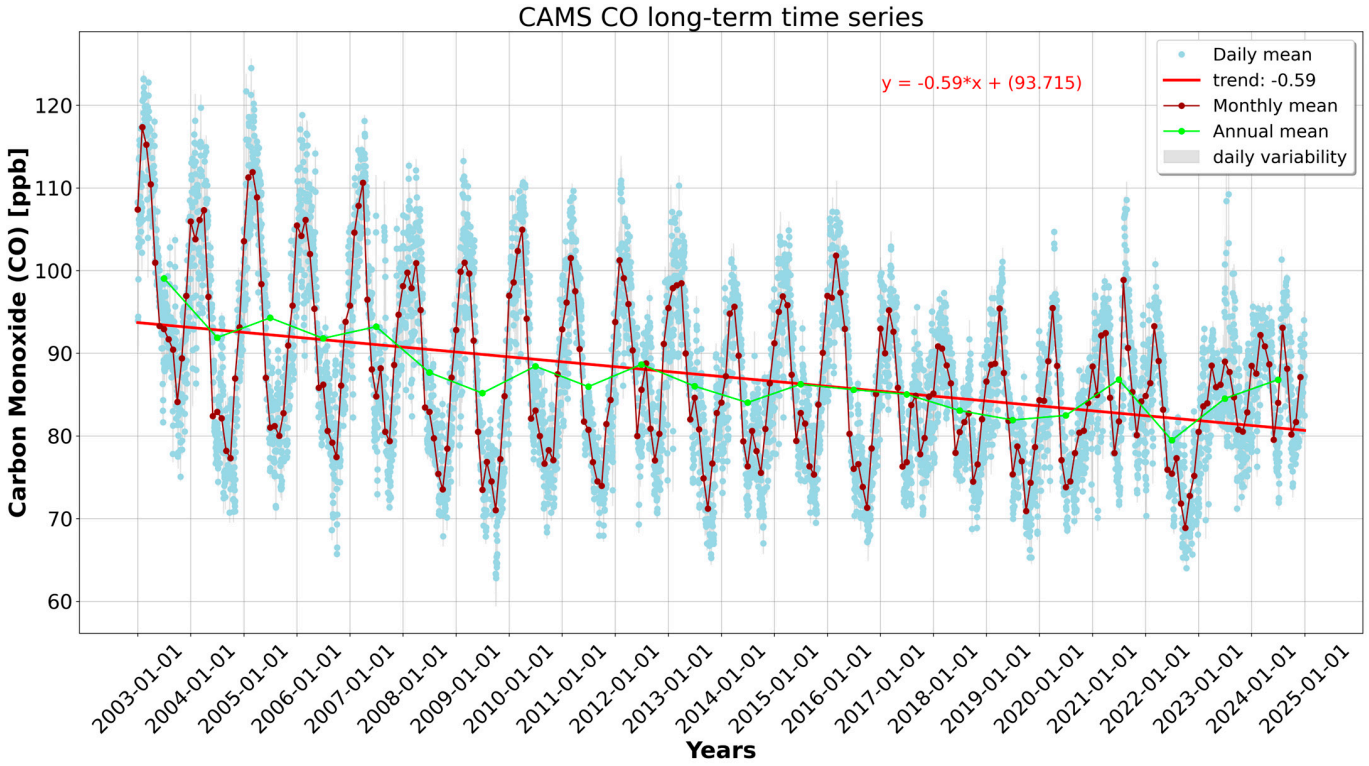

Figure 11. Long-term time series of total column concentrations of CO over Greece, covering the period 2003–2024. The red line shows the trend, while dark red and blue dots represent the monthly mean and daily mean concentrations, respectively.

To assess the spatial anomalies in carbon monoxide (CO) concentrations over Greece, a comparative analysis was performed between the year of interest and a reference period (2003–2013), as we already showed for the cases of CO_2 and CH_4. Specifically, the monthly mean CO concentrations were calculated for each month of both periods. The corresponding monthly mean for the year of interest was then computed, and relative

anomalies were derived as percentage deviations from the reference period, according to the following formula:

$$\Delta CO\ [\%]\ = \left(\left(CO_{year} - CO_{climatology} \right) / \left(CO_{climatology} \right) \right) * 100 \quad (3)$$

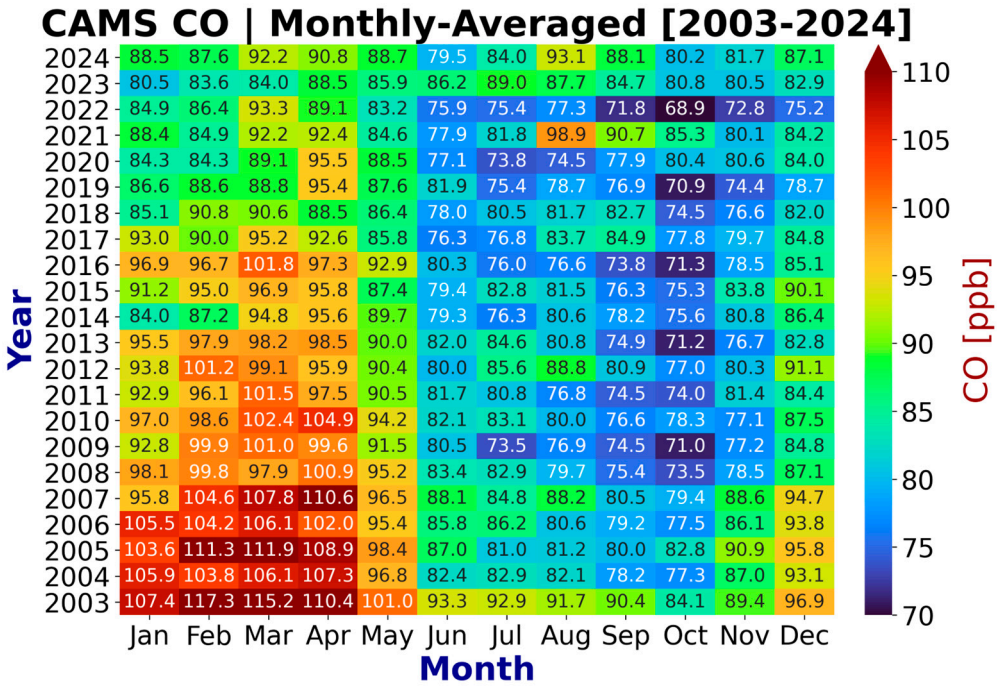

Figure 12. Monthly averaged heatmap of CO over Greece per year.

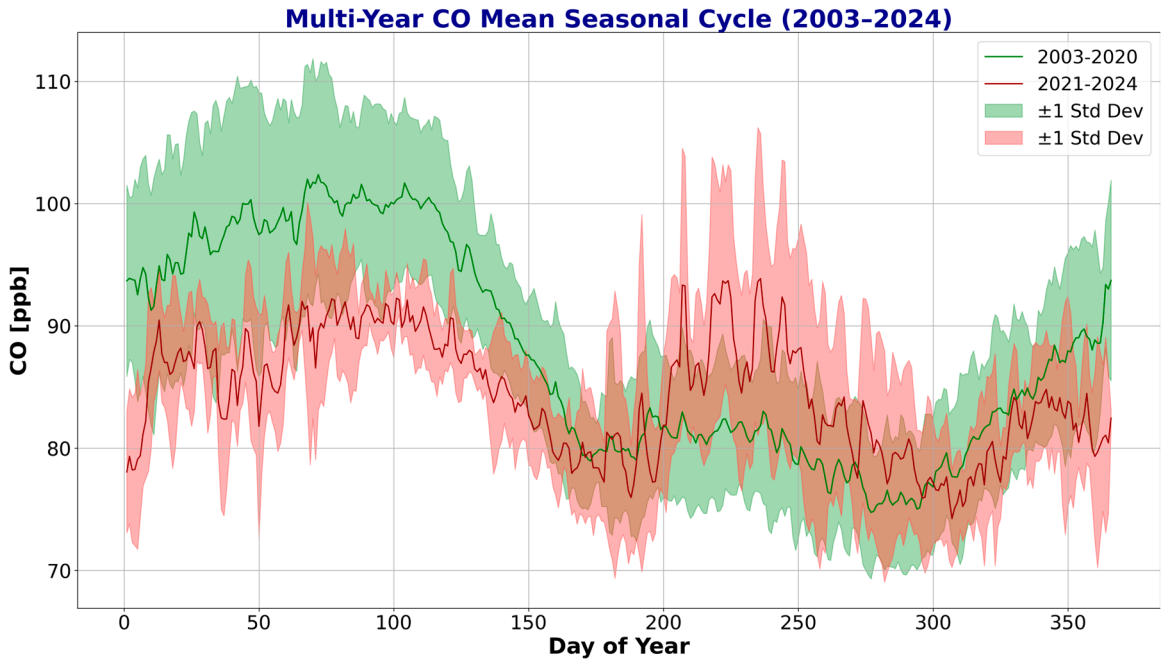

Figure 13. Seasonal cycle of CO daily mean concentrations over Greece. The red solid line and light red shadow represent the daily mean concentrations between 2021 and 2024, while the green ones cover the longer period between 2003 and 2020.

A negative CO anomaly was observed after 2008 during the winter period, while between 2018 and 2024 a negative anomaly exceeding 20% occurred during the winter and spring seasons. During the summers of 2021, 2023, and 2024, positive CO anomalies

were detected, driven by wildfire episodes (Figure 14). The largest anomaly occurred in August 2021, resulting from the extended fire events in northern Evia [19]. CAMS seasonal mean CO anomalies over Greece for 2024, relative to the reference period of 2003–2013, are shown in Figure 15. All seasons exhibit a positive trend, with CO concentrations showing a particularly notable increase during autumn, reaching approximately 20%. The average XCO levels measured over Thessaloniki using the EM27/SUN instrument from 2019 to 2023 range from 84.12 ± 2.62 ppb in 2020 to 116.54 ± 26.24 ppb in 2023. Typically, carbon monoxide concentrations during the summer months are expected to remain below 100 ppb, as observed in 2019, 2020, and 2022, due to lower anthropogenic emissions compared to other periods of the year [19].

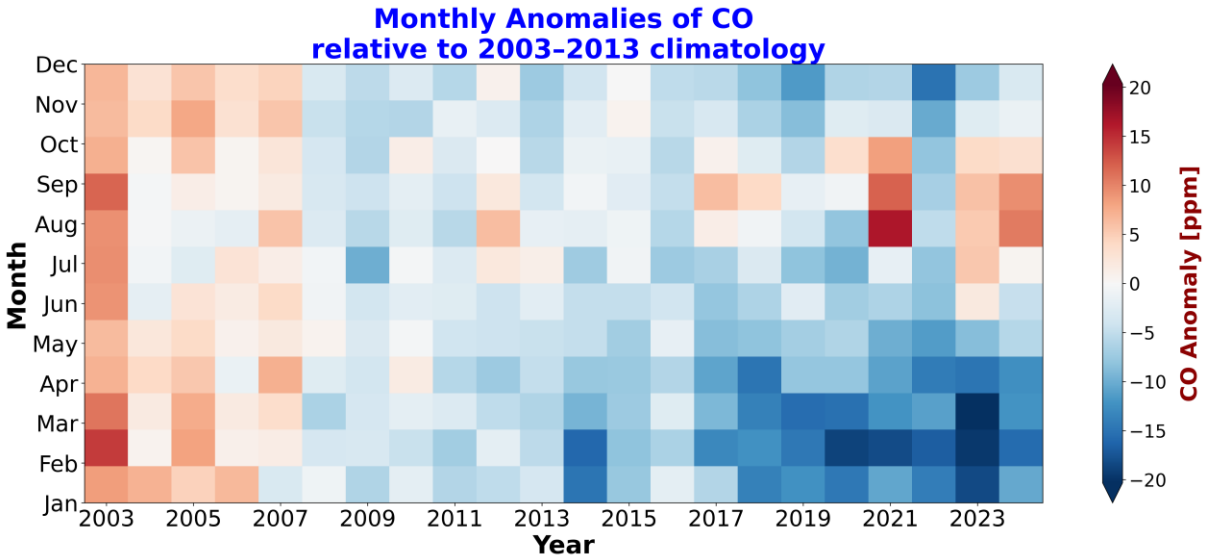

Figure 14. CO anomalies over Greece relative to the reference period, 2003–2013.

Within the framework of the present study, deviations in CO concentrations over Greece are examined, with particular emphasis on the impacts of wildfires over the past two decades. A comparative analysis was conducted between two distinct reference periods: 2003–2013 and 2014–2024. The analysis is based on the calculation of monthly CO anomalies, derived by subtracting the mean values of one period from those of the other on a monthly basis. The results indicate a reduction in anthropogenic CO emissions, particularly during the second period, while the seasonal variability of CO concentrations is increasingly influenced by summer wildfires, which appear to emerge as a key driver of variability in recent years (Figure 16a). Notably, the years 2021, 2023, and 2024 show the largest deviations from the reference period, with more pronounced enhancements during the summer months. In Figure 17, CAMS monthly mean CO anomalies are plotted together with the monthly mean wind speed derived from the CAMS EAC4 dataset. Winter and summer months were analyzed across multiple years to assess the impact of wildfire episodes on seasonal CO variability. Positive anomalies over Greece were identified in February 2002, whereas February 2021 and 2024 exhibited negative anomalies exceeding 20%. In 2007, elevated ΔCO values were observed in southwestern Greece, coinciding with wildfire activity and enhanced monthly mean wind conditions. Similarly, 2021 and 2024 revealed a marked increase in CO concentrations across the country, with monthly wind speeds consistently exceeding 7 m/s. Figure 18 presents the CAMS daily mean CO anomalies over Greece during the last decade compared to the total mean climatology, in terms of standard deviation, to identify the origin of the CO biomass burning emission

sources (>2σ) discussed previously in this paper. Figure S1 shows the relationship between CAMS monthly mean anomalies of ΔCH_4, ΔCO, and ΔOH.

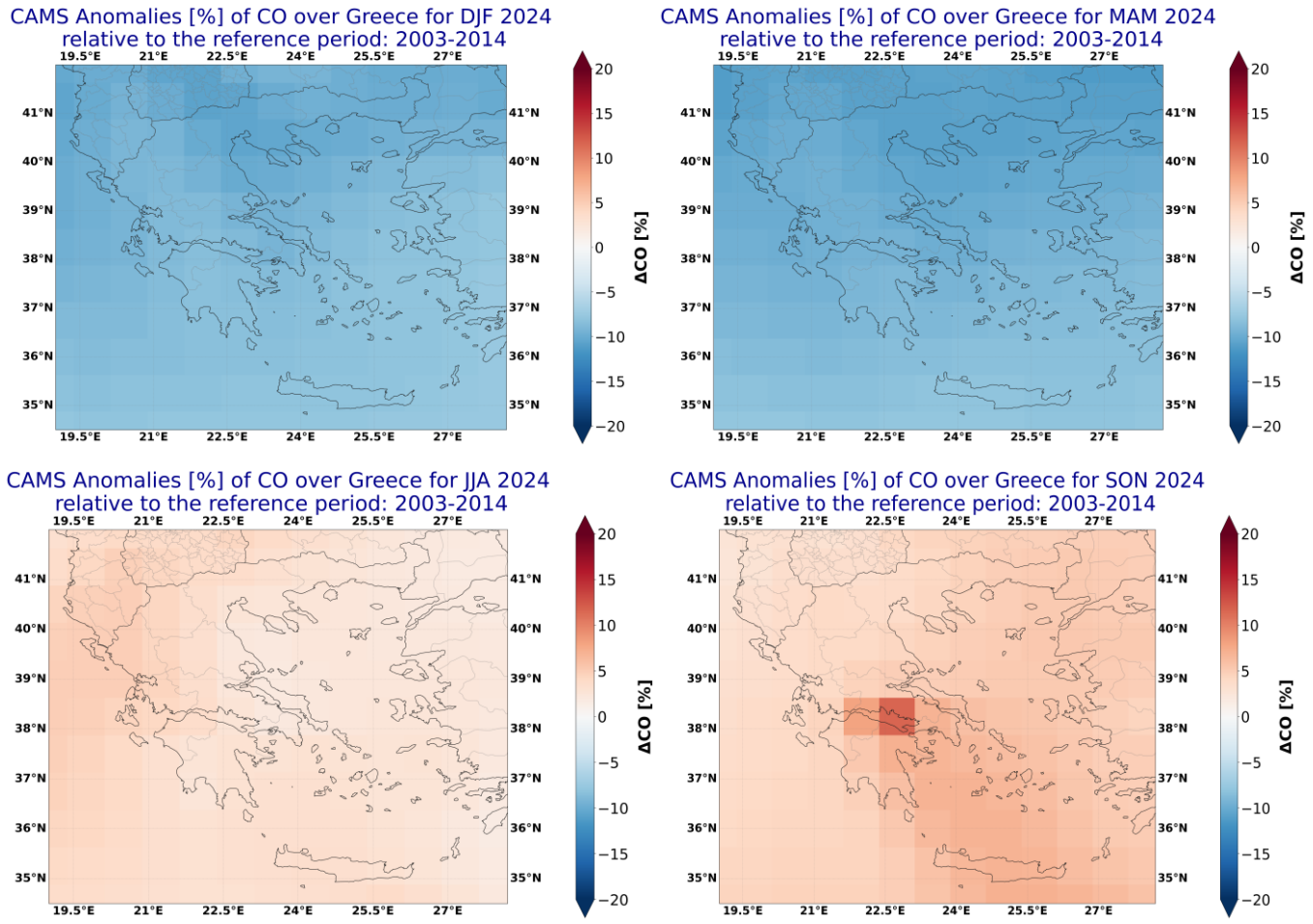

Figure 15. CAMS seasonal mean CO anomalies over Greece for 2024, relative to the reference period.

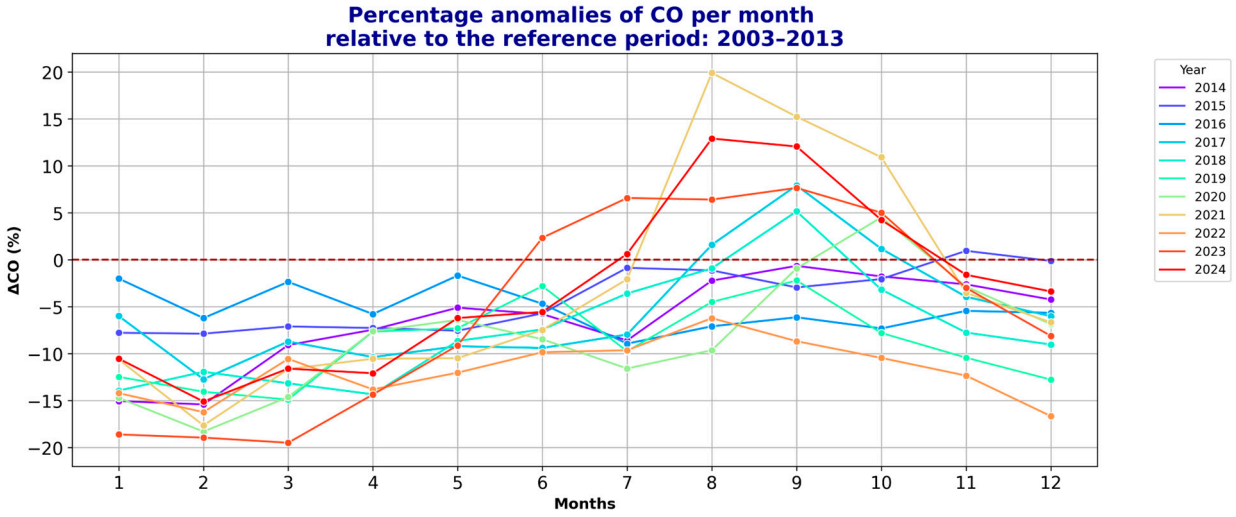

(**a**)

Figure 16. *Cont.*

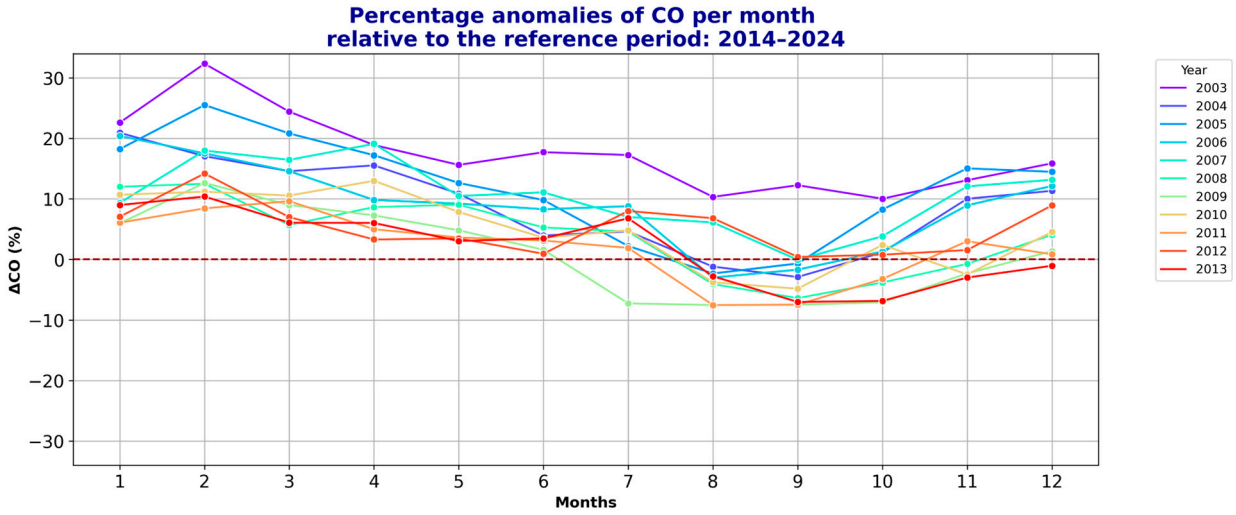

(**b**)

Figure 16. Percentage difference of monthly mean CO anomalies over Greece relative to the (**a**) 2003–2013 and (**b**) 2014–2024 time periods.

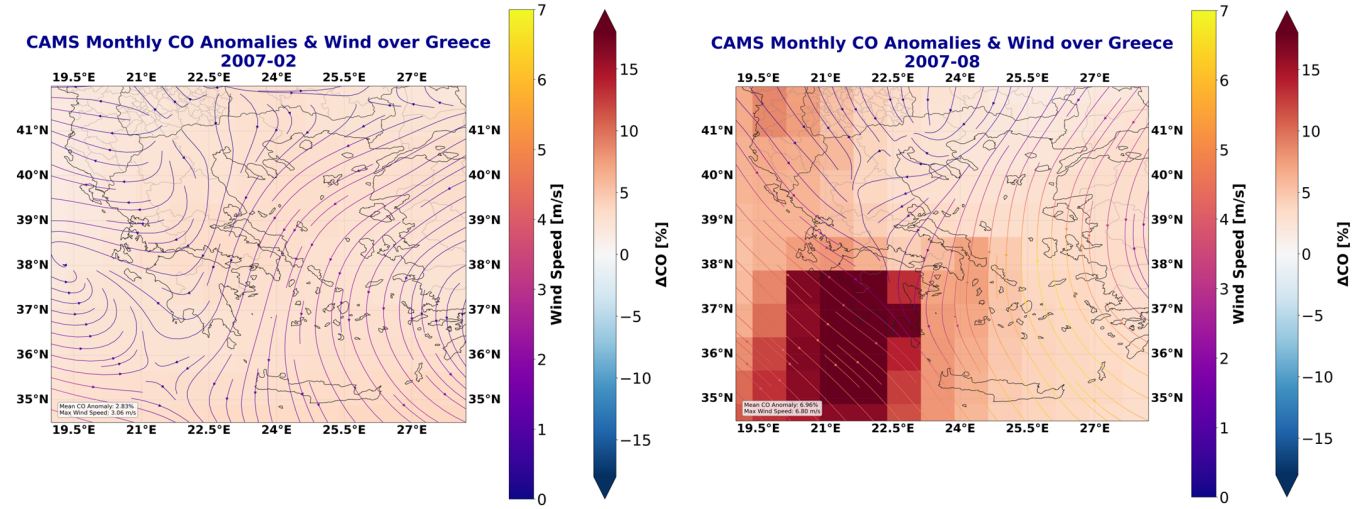

(**a**)

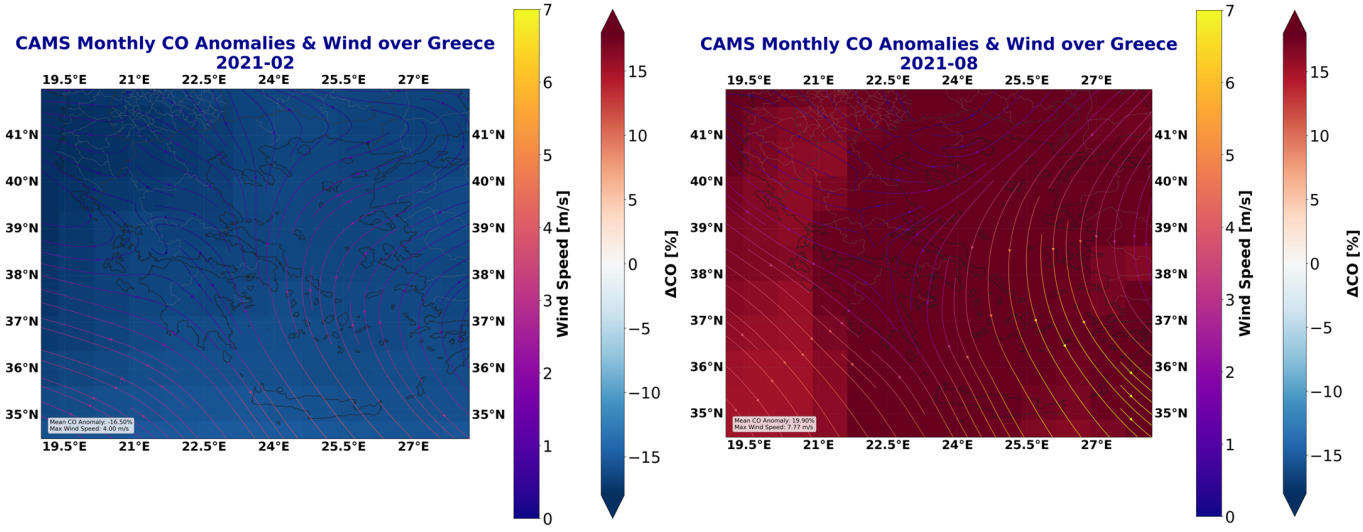

(**b**)

Figure 17. *Cont.*

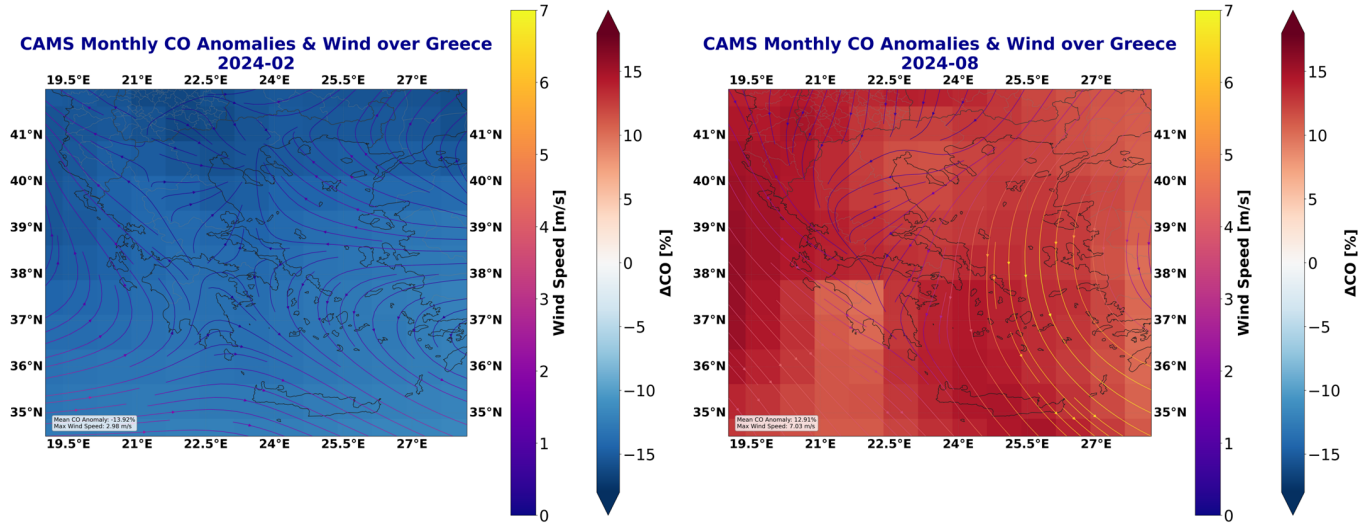

(**c**)

Figure 17. CAMS monthly averaged CO anomalies in February and August for (**a**) 2007, (**b**) 2021, and (**c**) 2024, plotted together with monthly mean wind speed and wind direction derived from the CAMS EAC4 dataset. The left color bar of each sub-plot represents the wind speed values, while the right one shows the ΔCO [%]. The legends in sub-plots show the mean CO anomaly [%] and the monthly mean wind speed in m/s.

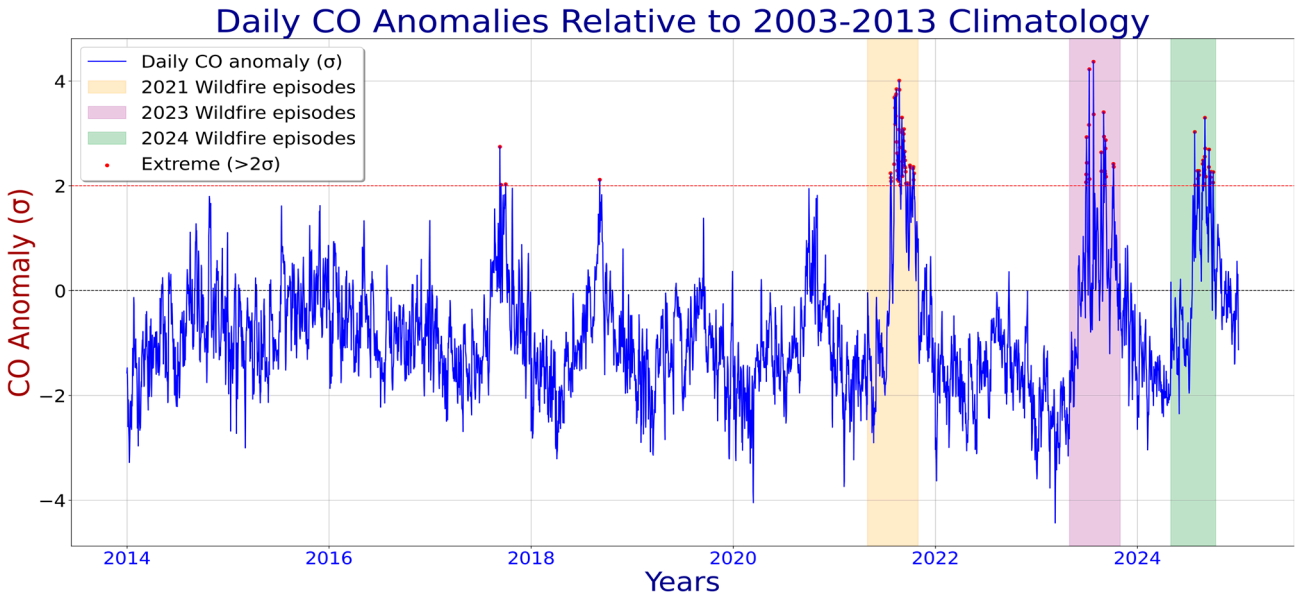

Figure 18. CAMS daily mean CO anomalies over Greece compared to the total mean climatology in terms of standard deviation (σ). Vertical shaded areas in the plot highlight time periods associated with prolonged wildfire episodes.

3.2. Short/Mid-Term Variability of GHGs

Figure S2 shows the (a) short-term and (b) mid-term variability of CO_2 in Greece using a centered rolling 14-day window and biweekly 3-h climatology, respectively. We observe a percentage of variability that ranges between ±0.5% for both enhancements and sinks of CO_2. During winter season in 2013, 2017, 2018, and 2020, increased CO_2 concentrations are found due to anthropogenic emission sources, while during late December of 2020 mid-term fluctuations of CO_2 reveal the highest ΔCO_2 value of over 1.2% using the approach of mid-term variations. ΔCH_4 values exhibit greater variability than that of CO_2, lying between ±2% (Figure S3). During the winters of 2020, 2022, and 2024,

elevated methane concentrations were observed, likely associated with industrial activities in major urban areas and natural gas exploitation. This behavior in CH_4 variability adheres to a consistent pattern of methane's different and various sources in many cities in Greece. In one study [19], CH_4 in Thessaloniki shows similar behavior during this period. Figure S4 shows the short/mid-term variability of CO in Greece. CO exhibits variability within a $\pm$10% range in both methods of analysis. However, due to its shorter atmospheric lifetime compared to CO_2 and CH_4, CO exhibits more pronounced episodic fluctuations, primarily driven by local anthropogenic sources such as industrial activity, transportation, and residential heating during the winter months. During the summer, wildfire events are responsible for the largest observed changes (ΔCO) in both directions, reflecting the short- and mid-term variability in CO concentrations associated with such episodic events. CAMS data effectively capture fire episodes in Greece, with the highest increases in CO concentrations observed during August 2007, associated with fires in Athens, and, in 2003, linked to fires in Alexandroupoli. In both cases, CO levels exceeded a 20% increase, highlighting the significant impact of these fire events on local air quality.

3.3. Long-Term Variability of GHGs

Figure S5 shows a more discernible picture of CO_2 variations compared to the previous methods. Higher ΔCO_2 values were observed during the late spring and winter seasons, with a notable influence from fire episodes on CO_2 concentrations, particularly during significant and prolonged wildfire events in Greece. Additionally, CO_2 variability shows a consistent upward trend from autumn 2018 to 2020, culminating in its highest recorded ΔCO_2 values, exceeding 5 ppm. When dividing the data by regions—northern, central, and southern Greece—we observe a similar pattern in CO_2 variations, with values ranging from +5 to $-$5 ppm, presented in the Supplementary Materials (Figure S8a–c). Regarding methane (Figure S6), we observe fluctuations in CH_4 concentrations around $\pm 1.5 \times 10^{16}$. During the winter and spring months, larger variability is observed, likely due to increased anthropogenic emissions, like fossil fuels, energy, natural gas, or mostly enteric fermentation in livestock and manure management. In autumn, elevated CH_4 concentrations are primarily attributed to agricultural activities, particularly in northern Greece. Additionally, in southern Greece (Figure S9c), we observe the lowest variability in CH_4 concentrations compared to northern and central Greece. The reduced variability observed in the southern region may be attributed to localized emission sources, which tend to smooth temporal fluctuations in CH_4 concentrations. Figure S7 illustrates the variations in CO concentrations across Greece, with a range of $\pm$20 ppb. In northern Greece (Figure S10a), we observe a CO increase of over 30 ppb during August 2007, reflecting the effect of wildfires in Athens, while Figure S10c shows an increase of CO concentrations of over 60%. It is remarkable how CO concentrations during the summer 2023 fire episodes in Alexandroupoli spread southward across central Greece, originating from the northeastern part of the country. This resulted in significant CO enhancements in southern Greece, with concentrations reaching—and, in some cases, exceeding—those observed in northern Greece, showing increases of over 50%. Due to the shorter atmospheric lifetime of CO compared to CO_2 and CH_4, it is more strongly affected by episodic events, as air mass transport can rapidly disperse CO across large areas of Greece.

While dividing Greece into northern, central, and southern regions highlights spatial patterns of GHG variability, the observed differences likely result from a combination of local emissions and transboundary transport. For example, elevated CO levels in southern and central Greece during wildfire episodes in northern and northeastern areas indicate the rapid influence of air mass transport, consistent with studies in the Mediterranean showing long-range dispersion of pollutants across regions [32]. Conversely, the lower

CH_4 variability in southern Greece suggests dominance of more localized sources, such as agriculture and livestock, which tend to produce steadier emissions. Integrating both local and regional influences provides a more comprehensive explanation for the observed patterns, emphasizing that seasonal and episodic events interact with atmospheric circulation to shape the spatial variability of GHGs across Greece.

In Figures S11 and S12, geographical maps of ΔCO_2 and ΔCH_4 over Greece are presented. In Figure S13, we present four cases of air mass transport of CO across Greece, highlighting the enhanced CO concentrations during intense fire episodes.

3.4. CAMS Emission Inventories and GHG Fluxes over Greece

This study employs two complementary datasets from the Copernicus Atmosphere Monitoring Service (CAMS) to characterize greenhouse gas emissions over Greece. First, we use the CAMS Global Emission Inventories, which provide sector-resolved anthropogenic emissions of CO_2, CH_4, and CO at monthly temporal resolution. These inventories report surface emission fluxes in units of kg/m^2/s,, representing monthly mean emission rates within each model grid cell. Emission fluxes were converted into monthly integrated emissions (kg $\times$ m^{-2} $\times$ month^{-1}) by multiplying each monthly mean flux by the exact number of seconds in the corresponding month.

In addition to the emission inventories, the CAMS global inversion-optimized greenhouse gas fluxes dataset is used, providing optimized CO_2 and CH_4 surface fluxes derived from atmospheric inversion systems that assimilate satellite observations. We present sector-specific time series of CO_2 and CH_4 to assess monthly variability, quantify the relative contributions of major emission sectors, and identify patterns associated with anthropogenic activity. They were multiplied by the grid cell area to convert them into emission rates (kg $\times$ month^{-1}) and plotted as monthly values in the time series shown in the figures below. Furthermore, spatial emission maps were generated for CO_2, CH_4, and CO, highlighting the geographical distribution of emission rates and the influence of key emitting sectors. These maps provide insight into regional emission hotspots and the spatial heterogeneity associated with different source categories. In Figure 19, CAMS fossil CO_2 emissions show a discernible seasonality with higher emission rates during winter and autumn, while they drop to lower rates during summer, when lower anthropogenic emissions occur. A decline is observed from 2018 to 2020, followed by a period of relative stability, with the highest emission rates occurring in January 2024 and 2025. Fossil emissions are out of phase with surface ocean fluxes, which show a constant seasonal variation over the years, with lower emission rates occur during winter (Figure 19). Land surface emission rates are highly variable between months, with negative values (<2 kg/month) after spring of 2020. Seasonal variation in fossil CO_2 emissions over Greece largely reflects underlying changes in energy demand and socioeconomic activity. Emissions increase during winter due to heating requirements, while in summer elevated temperatures and tourism-driven electricity demand contribute to higher emission levels. In addition, mobility and transport activity—including road traffic, aviation, and, in particular, Greece's highly seasonal maritime sector—further amplify summer emission peaks.

In the following maps (Figure 20), CAMS fossil emission rates are presented over Greece, comparing January 2015 with 2024. We observe higher emissions over Athens, central Greece, and west of Thessaloniki, where most anthropogenic emission sources occur.

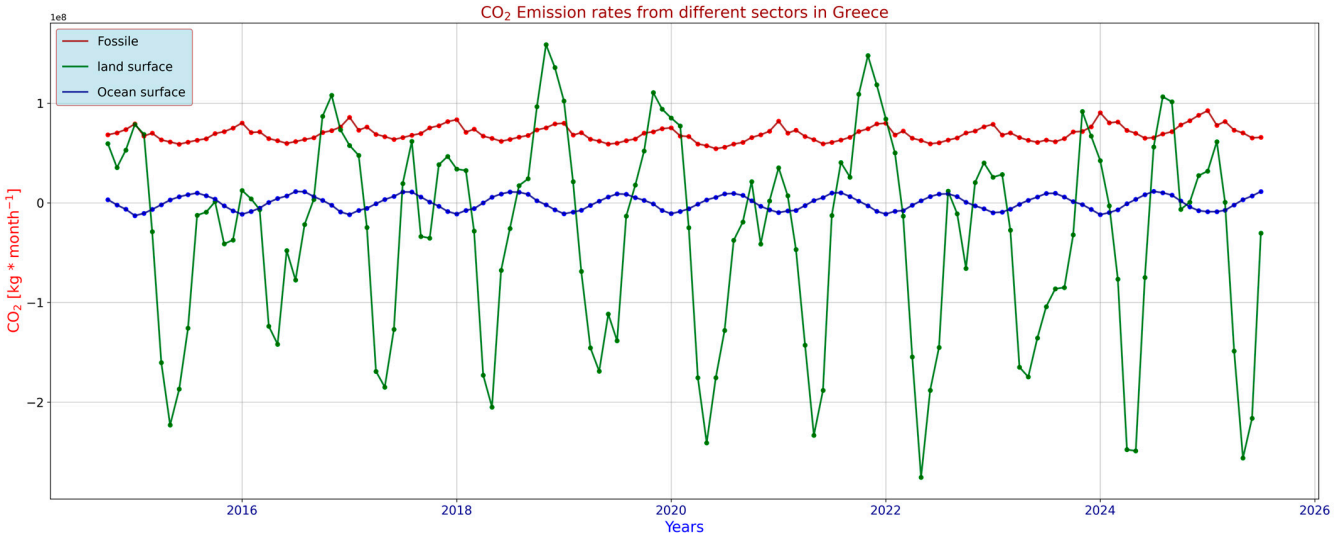

Figure 19. Fossil emission rate of CO_2 for fossil, land, and ocean surface over Greece.

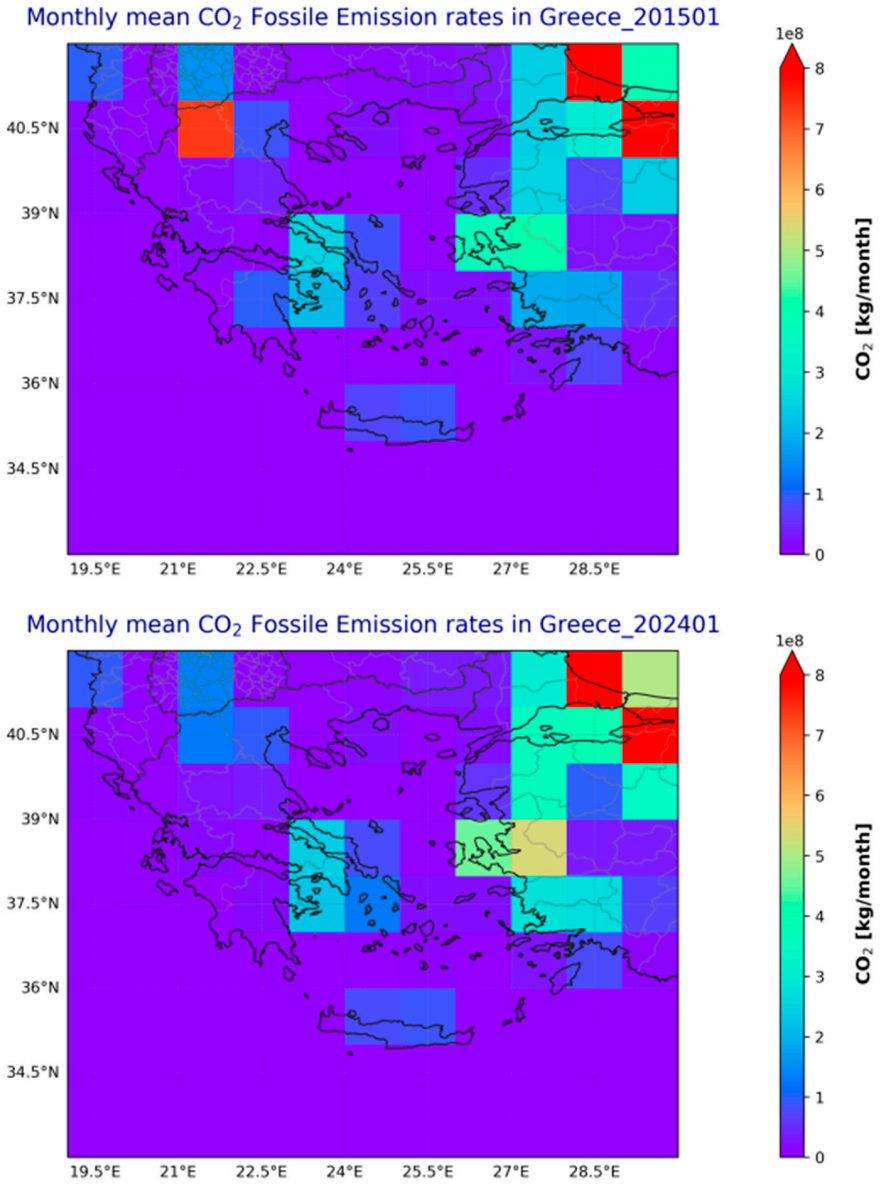

Figure 20. Maps of monthly mean CO_2 emission rates over Greece during January of 2015 and 2024.

Monthly mean emission rates of CH_4 from different sources in Greece are shown in Figure 21. Wetlands, rice cultivation, and biomass burning sectors are analyzed in this study. Figure 21 shows the time series of these CH_4 emission sources. Wetlands exhibit the highest monthly variability and the greatest emission rates compared to the other sources. As one of the most significant methane emission sources in Greece, wetlands show a consistent seasonal pattern across years, with the majority of emissions occurring during autumn and winter. High variability is observed, with notable increases during late spring and a sharp rise during the summer of 2018. CAMS rice-related CH_4 emissions in Greece exhibit a clear seasonal cycle, with elevated emissions from summer to autumn, consistent with typical rice-growing and post-harvest periods. Biomass burning emission rates show higher values during the summer period related to the fire episodes in 2021, 2023, and 2024. Figure 22 shows monthly mean CH_4 emissions from the biomass burning sector during summer 2021 and 2023, when major fire episodes occurred in Athens and Alexandroupoli.

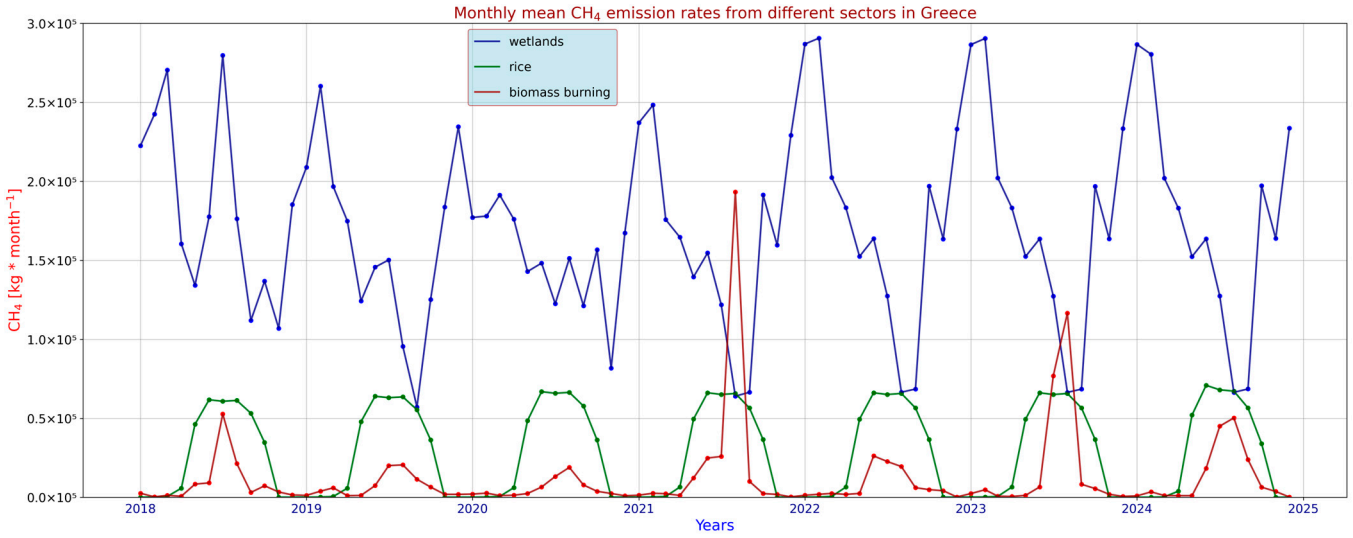

Figure 21. Monthly averaged CH_4 emission rates over Greece from wetlands, rice, and biomass burning.

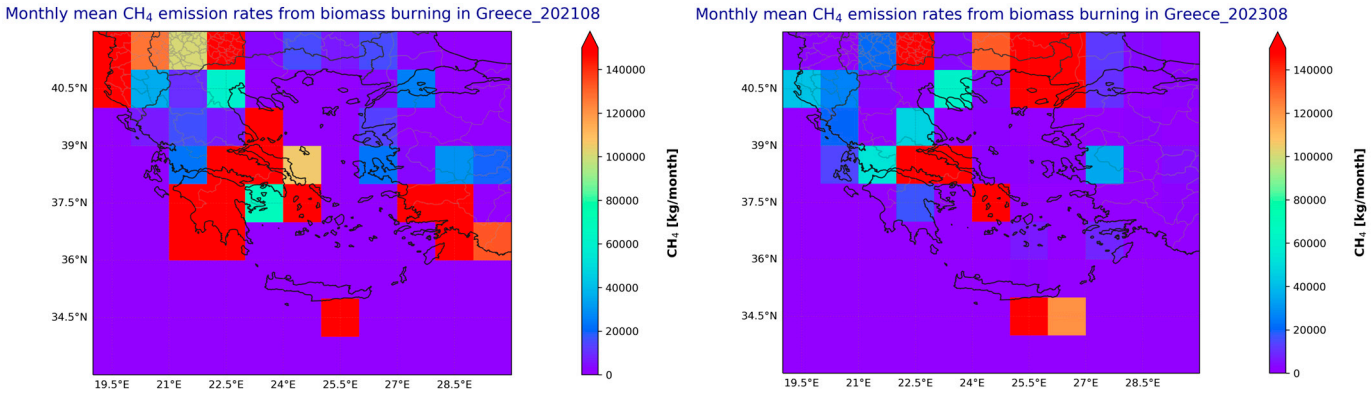

Figure 22. Maps of monthly mean CH_4 emission rates over Greece from the biomass burning sector.

4. Discussion

To sum up, both CO_2 and CH_4 exhibit a clear, positive, long-term trend and a pronounced seasonal cycle. In contrast, CO follows a different pattern, showing an overall negative trend, while wildfire events are responsible for the highest CO enhancements observed over the years. CO_2 and CO share common sources related to fossil fuel combustion, whereas methane has a strong contribution from agricultural activities. An increase in CO

concentrations may increase methane's lifetime by decreasing the oxidizing capacity of hydroxyl radicals (OH), especially during summer. Wildfire episodes trigger this co-variability and affect OH's lifetime and its ability to oxidize methane, increasing GHG's lifetime as a consequence. During periods of intense biomass burning, natural emissions can far exceed anthropogenic sources, leading to sharp increases in tropospheric CO concentrations. These emissions affect air quality not only locally but also on a regional to global scale, as CO can be transported over long distances through atmospheric circulation and detected from the surface up to the upper troposphere and even the stratosphere under favorable conditions. In May 2025, extensive wildfires in Canada produced large amounts of CO that were transported across the Atlantic and reached southeastern Europe. CAMS global greenhouse gas forecasts [33], which consist of a horizontal resolution of $0.1^\circ \times 0.1^\circ$ and a vertical resolution of 137 model levels and 25 pressure levels, recorded elevated CO levels over Greece, highlighting the transboundary and intercontinental transport of fire-related pollutants. Similar events were observed in the summer of 2023, confirming the ability of pyrogenic emissions to travel thousands of kilometers through upper-tropospheric and stratospheric pathways. Figure S14 illustrates CO concentrations over Greece associated with long-range transport of wildfire emissions. Panel (a) shows increased CO concentrations during the transport of air masses from the Manitoba wildfires to Europe on 19 May, as depicted by CAMS data at 300 hPa. Panel (b) shows the transport of air masses from Russia to Greece in early June 2025, resulting in enhanced CO concentrations at 250 hPa. The information summarized in Tables S1–S3 provides an overview of the annual and seasonal mean differences in GHGs relative to the reference period of 2003–2013. In particular, Table S1 presents the CAMS annual mean differences in GHGs, Table S2 shows the seasonal mean percentage differences for 2020 (ΔCO_2) and 2024 (ΔCH_4 and ΔCO), and Table S3 compares CO anomalies for the periods of 2005–2007 and 2021–2024 across January–February and July–August.

GHG variability in Greece reveals clear seasonal and episodic patterns driven by both anthropogenic activities and natural events. Carbon dioxide shows relatively small short- and mid-term variability, with wintertime increases linked to anthropogenic emissions such as heating and urban activity, while occasional larger fluctuations are associated with extended fire episodes. Methane exhibits greater variability than CO_2, reflecting its diverse emission sources, including industrial activity, urban emissions, and agricultural processes. Carbon monoxide demonstrates the largest short-term variability and strong sensitivity to local emission sources. However, the most pronounced CO enhancements occur during summer wildfire events, which can rapidly influence air quality across large areas through atmospheric transport. Overall, the results highlight the combined influence of seasonal human activities, regional emission sources, and extreme events such as wildfires in shaping greenhouse gas variability across Greece.

Global GHG emissions from anthropogenic activities have steadily increased since 1990, with carbon dioxide representing the dominant contribution to total emissions, followed by methane, largely driven by sectors such as power generation, transportation, fuel exploitation, and agriculture [34]. In contrast, Greece shows a long-term decline in several greenhouse gas emissions, particularly CO_2, mainly due to reductions in the energy and industrial sectors, although road transport remains a significant and increasing source of CO_2 emissions [35]. Carbon monoxide emissions in Greece have also substantially decreased over the last decades, largely reflecting improvements in the transport and energy sectors [35]. CH_4 emissions display a more complex pattern, with waste management representing the largest anthropogenic source, followed by agricultural activities such as enteric fermentation and rice cultivation, while the energy sector contributes a smaller share [35]. Although agricultural methane emissions have generally declined since 1990,

some sources—particularly waste-related emissions—have increased, highlighting the continued importance of waste management and agricultural practices in shaping CH_4 emissions in Greece [35]. The EDGAR report in 2024 reported declining GHG emissions after 2008 according to various emission sectors in Greece, which is in line with CO_2 and CH_4 emissions in Greece reported by the CAMS model. In Greece, power generation, transport, and industrial combustion and processes drive GHG emissions. Transport emissions were found to be 16% higher in 2023 compared to 1990; however, they were 20% lower compared to 2005. In Greece, total GHG emissions decreased by 46% in 2023 compared to 2005 according to [34].

In summary, CAMS GHG emission rates are in good agreement with those reported in the latest Greek National Report and are also consistent with the emission trends reported by the European Commission's Joint Research Centre in the EDGAR database, providing additional confidence in reported emission reductions and their relevance for policy evaluation. The road transportation sector shows a decrease in emissions for all categories, while agricultural activities drive methane emissions in Greece, as reported in [12].

5. Conclusions

This study examined the long-term trends, seasonal variability, and short-term dynamics of CO_2, CH_4, and CO over Greece using CAMS reanalysis data. The results show a clear increasing trend in CO_2 and CH_4 concentrations [19], consistent with global patterns, while CO exhibits an overall decreasing trend. However, episodic enhancements in CO are strongly linked to wildfire events, highlighting their impact on regional air quality and atmospheric composition. Despite this general decline, wildfire events were identified as a major driver of episodic CO enhancements, producing the highest observed concentrations and significantly affecting regional air quality [36,37]. The rise in CO levels influences methane's atmospheric lifetime by reducing the oxidizing capacity of hydroxyl radicals (OH), and this effect was found to be particularly prominent in summer [38,39]. Wildfire episodes can further enhance this co-variability, while evidence from the COVID-19 period suggests that reductions in anthropogenic emissions also weakened OH, limiting methane oxidation and contributing to increased CH_4 lifetimes [40]. Multi-scale variability analyses revealed distinct patterns in greenhouse gas behavior. Short- and mid-term analyses indicate relatively small fluctuations in CO_2 and CH_4 concentrations, whereas CO exhibits substantially larger variability, reflecting its responsiveness to episodic events and local emission sources.

The study also examined sectoral emission patterns in Greece. Fossil CO_2 emissions are strongly seasonal, with higher rates during winter and autumn, while methane emissions display distinct sector-dependent variability, particularly from wetlands, agricultural activities, and rice cultivation. Biomass burning associated with wildfire events represents an important episodic source affecting atmospheric composition during summer months. Greece has made notable progress in reducing greenhouse gas (GHG) emissions, achieving, approximately, a 35% reduction from 1990 levels by 2023 [35]. While this decline reflects effective measures in the energy and industrial sectors, current policies are projected to deliver only a 45–50% reduction by 2030, falling short of the legally binding 55% target. Consequently, although Greece is advancing toward its climate goals, additional measures—particularly in transport, buildings, and fossil fuel phase-out—are needed to align fully with its 2030 and 2050 climate commitments. From a policy perspective, the consistency between Copernicus Atmosphere Monitoring Service (CAMS), EDGAR, and national inventory data provides increased confidence in the reported downward trends in GHG emissions in Greece. These trends suggest that the country is making substantial progress toward its commitments under the European Union climate framework. These

findings are consistent with multiple datasets, including CAMS, EDGAR, and national inventories, which increases confidence in the observed downward trends in Greece's GHG emissions [41,42]. Despite this progress, projections indicate a potential overshoot relative to the 2030 and 2050 targets, particularly due to persistent emissions in the transport and agricultural sectors [41,43].

Supplementary Materials: The following supporting information can be downloaded at https://www.mdpi.com/article/10.3390/atmos17040392/s1. Figure S1. CAMS monthly mean CO anomalies for CH_4, CO and OH during intense wildfires in Greece. Figure S2. (a) Short-term and (b) mid-term variability of CO_2 in Greece using a centered rolling 14-day window and biweekly 3-hourly climatology respectively. Figure S3. (a) Short-term and (b) mid-term variability of CH_4 in Greece using a centered rolling 14-day window and biweekly 3-hourly climatology respectively. Figure S4. (a) Short-term and (b) mid-term variability of CO in Greece using a centered rolling 14-day window and biweekly 3-hourly climatology respectively. Figure S5. Long-term variability of CO_2 in Greece after detrended time series. The blue dots show the 3-hourly binned data, while the orange line shows the weekly averaged values. Figure S6. Long-term variability of CH_4 in Greece after detrended time series. The blue dots show the 3-hourly binned data, while the orange line shows the weekly averaged values. Figure S7. Long-term variability of CO_2 in Greece after detrended time series. The blue dots show the 3-hourly binned data, while the orange line shows the weekly averaged values. Figure S8. Detrended variability of CO_2 over (a) Northern, (b) Central and (c) Southern Greece. Figure S9. Detrended variability of CH_4 over (a) Northern, (b) Central and (c) Southern Greece. Figure S10. Detrended variability of CO over (a) Northern, (b) Central and (c) Southern Greece. Figure S11. Maps of CO_2 variability using a biweekly 3-hourly climatology, captured above Greece. Figure S12. Maps of CH_4 variability using a biweekly 3-hourly climatology, captured above Greece. Figure S13. The maps above show the course of high enhanced CO concentrations as a result of extended wildfire episodes in Greece during (a) August-2021, (b) August-2023, as well as in (c) early October-2024. Figure S14. (a) Increased concentrations of CO over Greece during the transport of air masses from the Manitoba wildfires toward Europe on 19 May, as depicted by data from the Copernicus Atmosphere Monitoring Service (CAMS) at 300 hPa. (b) Transport of air masses from Russia to Greece in June 2025, which resulted in elevated CO concentrations at 250 hPa. Figure S15. CAMS monthly mean maps of CO_2 surface emission fluxes from industrial sector in Greece. Figure S16. CAMS monthly mean maps of CO_2 surface emission fluxes from residential sector in Greece. Figure S17. CAMS monthly mean maps of CO_2 surface emission fluxes from road transportation in Greece. Figure S18. CAMS monthly mean maps of CO surface emission fluxes from industry in Greece. Figure S19. CAMS monthly mean maps of CO surface emission fluxes from residential sector in Greece. Figure S20. CAMS monthly mean maps of CO surface emission fluxes from road transportation in Greece. Figure S21. CAMS monthly mean maps of CH_4 surface emission fluxes from agriculture-livestock in Greece. Figure S22. CAMS monthly mean maps of CH_4 surface emission fluxes from agriculture-soils in Greece. Figure S23. CAMS monthly mean maps of CH_4 surface emission fluxes from waste burning in Greece. Table S1. CAMS annual mean differences in GHGs relative to the reference period 2003–2013. Table S2. CAMS seasonal mean percentage differences in GHGs compared to the reference period of 2003–2013. ΔCH_4 and ΔCO are calculated for 2024, while ΔCO_2 for 2020. Table S3. CO anomalies [%] relative to the reference period 2003–2013, comparing the periods 2005–2007 and 2021–2024 for January–February, and July–August.

Author Contributions: Conceptualization, M.M., V.A. and S.K.; investigation, M.M., V.A., S.K. and A.K.; methodology, M.M., A.K. and S.K.; resources, M.M., S.K., A.K., V.A. and J.K.; data curation, M.M. and J.K.; formal analysis, M.M.; supervision, V.A.; writing—original draft, M.M. and V.A.; writing—review and editing, V.A., A.K., S.K. and J.K. All authors have read and agreed to the published version of the manuscript.

Funding: This project has received funding from the LandShift project by the European Union's Horizon Europe Research and Innovation Programme (HORIZON-CL6-2024-CLIMATE-01-4) under Grant Agreement No 101182007.

Institutional Review Board Statement: Not applicable.

Informed Consent Statement: Not applicable.

Data Availability Statement: The CAMS data are available from https://ads.atmosphere.copernicus.eu/datasets (accessed on 17 December 2025).

Acknowledgments: We acknowledge the Copernicus Atmosphere Monitoring Service (CAMS) Data Store (https://ads.atmosphere.copernicus.eu/datasets, accessed on 17 December 2025) for the usage of their data. Furthermore, we gratefully acknowledge the support provided by the CAMS National Collaboration Programme (NCP) by ECMWF. The authors acknowledge "LandShift": Community-Led Creation of Living Spaces in Shifting Landscapes for Climate-Resilient Land Use Management and Supporting the New European Bauhaus.

Conflicts of Interest: The authors declare no conflicts of interest.

References

1. Jackson, R.B.; Saunois, M.; Martinez, A.; Canadell, J.G.; Yu, X.; Li, M.; Poulter, B.; Raymond, P.A.; Regnier, P.; Ciais, P.; et al. Human activities now fuel two-thirds of global methane emissions. *Environ. Res. Lett.* **2024**, *19*, 101002. [CrossRef]
2. Saunois, M.; Martinez, A.; Poulter, B.; Zhang, Z.; Raymond, P.A.; Regnier, P.; Canadell, J.G.; Jackson, R.B.; Patra, P.K.; Bousquet, P.; et al. Global Methane Budget 2000–2020. *Earth Syst. Sci. Data* **2025**, *17*, 1873–1958. [CrossRef]
3. Griffin, D.; Chen, J.; Anderson, K.; Makar, P.; McLinden, C.A.; Dammers, E.; Fogal, A. Biomass burning CO emissions: Exploring insights through TROPOMI-derived emissions and emission coefficients. *Atmos. Chem. Phys.* **2024**, *24*, 10159–10186. [CrossRef]
4. Dils, B.; Cui, J.; Henne, S.; Mahieu, E.; Steinbacher, M.; De Mazière, M. 1997–2007 CO trend at the high Alpine site Jungfraujoch: A comparison between NDIR surface in situ and FTIR remote sensing observations. *Atmos. Chem. Phys.* **2011**, *11*, 6735–6748. [CrossRef]
5. Spivakovsky, C.M.; Logan, J.A.; Montzka, S.A.; Balkanski, Y.J.; Foreman-Fowler, M.; Jones, D.B.A.; Horowitz, L.W.; Fusco, A.C.; Brenninkmeijer, C.A.M.; Prather, M.J.; et al. Three-dimensional climatological distribution of tropospheric OH: Update and evaluation. *J. Geophys. Res. Atmos.* **2000**, *105*, 8931–8980. [CrossRef]
6. Thompson, A.M. The Oxidizing Capacity of the Earth's Atmosphere: Probable Past and Future Changes. *Science* **1992**, *256*, 1157–1165. [CrossRef]
7. Lelieveld, J.; Gromov, S.; Pozzer, A.; Taraborrelli, D. Global tropospheric hydroxyl distribution, budget and reactivity. *Atmos. Chem. Phys.* **2016**, *16*, 12477–12493. [CrossRef]
8. IEA. *World Energy Outlook 2021*; IEA: Paris, France, 2021. Available online: https://www.iea.org/reports/world-energy-outlook-2021 (accessed on 11 February 2026).
9. Lan, X.; Thoning, K.W.; Dlugokencky, E.J. Trends in Globally-Averaged CH_4, N_2O, and SF_6 Determined from NOAA Global Monitoring Laboratory Measurements. Version 2025-11. 2022. Available online: https://doi.org/10.15138/P8XG-AA10 (accessed on 8 April 2026). [CrossRef]
10. World Meteorological Organization. The State of Greenhouse Gases in the Atmosphere Based on Global Observations Through 2024. *Greenhouse Gas Bulletin*, 16 October 2025; No. 21. Available online: https://wmo.int/sites/default/files/2025-10/GHG-21_en.pdf (accessed on 11 February 2026).
11. Doc, J.; Bréon, F.-M.; Lopez, M.; Té, Y.; Jeseck, P.; Lian, J.; Nief, G.; Parent, A.; Leuridan, H.; Ramonet, M. Two years of total column measurements of CO_2, CH_4 and CO in Paris, France. *EGUsphere* **2025**, *2025*, 1–32. [CrossRef]
12. Mermigkas, M.; Topaloglou, C.; Balis, D.; Koukouli, M.E.; Hase, F.; Dubravica, D.; Borsdorff, T.; Lorente, A. FTIR Measurements of Greenhouse Gases over Thessaloniki, Greece in the Framework of COCCON and Comparison with S5P/TROPOMI Observations. *Remote Sens.* **2021**, *13*, 3395. [CrossRef]
13. Hase, F.; Frey, M.; Kiel, M.; Blumenstock, T.; Harig, R.; Keens, A.; Orphal, J. Addition of a channel for XCO observations to a portable FTIR spectrometer for greenhouse gas measurements. *Atmos. Meas. Tech.* **2016**, *9*, 2303–2313. [CrossRef]
14. Tu, Q.; Hase, F.; Blumenstock, T.; Kivi, R.; Heikkinen, P.; Sha, M.K.; Raffalski, U.; Landgraf, J.; Lorente, A.; Borsdorff, T.; et al. Intercomparison of atmospheric CO_2 and CH_4 abundances on regional scales in boreal areas using Copernicus Atmosphere monitoring Service (CAMS) analysis, COllaborative Carbon Column observing Network (COCCON) spectrometers, and Sentinel-5 Precursor satellite observations. *Atmos. Meas. Tech.* **2020**, *13*, 4751–4771. [CrossRef]
15. Alberti, C.; Hase, F.; Frey, M.; Dubravica, D.; Blumenstock, T.; Dehn, A.; Castracane, P.; Surawicz, G.; Harig, R.; Baier, B.C.; et al. Improved calibration procedures for the EM27/SUN spectrometers of the COllaborative Carbon Column Observing Network (COCCON). *Atmos. Meas. Tech.* **2022**, *15*, 2433–2463. [CrossRef]

16. Mermigkas, M.; Topaloglou, C.; Koukouli, M.-E.; Balis, D.; Hase, F.; Dubravica, D.; Borsdorff, T.; Lorente, A. Sentinel-5P/TROPOspheric Monitoring Instrument CH_4 and CO Total Column Validation over the Thessaloniki Collaborative Carbon Column Observing Network Site, Greece. *Environ. Sci. Proc.* **2023**, *26*, 188. [CrossRef]
17. Bougiatioti, A.; Gialesakis, N.; Sarafidis, Y.; Gini, M.I.; Mermigkas, M.; Kalkavouras, P.; Mirasgedis, S.; Ramonet, M.; Narbaud, C.; Lopez, M.; et al. Sources and Variability of Greenhouse Gases over Greece. *Atmosphere* **2024**, *15*, 1288. [CrossRef]
18. Buchholz, R.R.; Worden, H.M.; Park, M.; Francis, G.; Deeter, M.N.; Edwards, D.P.; Emmons, L.K.; Gaubert, B.; Gille, J.; Martínez-Alonso, S.; et al. Air pollution trends measured from Terra: CO and AOD over industrial, fire-prone, and background regions. *Remote Sens. Environ.* **2021**, *256*, 112275. [CrossRef]
19. Mermigkas, M.; Topaloglou, C.; Balis, D.; Hase, F.; Dubravica, D. Local and regional enhancements of GHGs in Thessaloniki, inferred from ground-based FTIR measurements. *Atmos. Res.* **2025**, *319*, 108035. [CrossRef]
20. Mermigkas, M.; Kartsios, S.; Kampouri, A.; Drosoglou, T.; Amiridis, V. Variability and Long-Term Trends of CO_2 & CH_4 in European Countries, Using CAMS Global Reanalysis Data. *Environ. Earth Sci. Proc.* **2025**, *35*, 4. [CrossRef]
21. Agustí-Panareda, A.; Barré, J.; Massart, S.; Inness, A.; Aben, I.; Ades, M.; Baier, B.C.; Balsamo, G.; Borsdorff, T.; Bousserez, N.; et al. Technical note: The CAMS greenhouse gas reanalysis from 2003 to 2020. *Atmos. Chem. Phys.* **2023**, *23*, 3829–3859. [CrossRef]
22. Inness, A.; Ades, M.; Agustí-Panareda, A.; Barré, J.; Benedictow, A.; Blechschmidt, A.-M.; Dominguez, J.J.; Engelen, R.; Eskes, H.; Flemming, J.; et al. The CAMS reanalysis of atmospheric composition. *Atmos. Chem. Phys.* **2019**, *19*, 3515–3556. [CrossRef]
23. Granier, C.; Darras, S.; van der Gon, H.D.; Doubalova, J.; Elguindi, N.; Galle, B.; Gauss, M.; Guevara, M.; Jalkanen, J.-P.; Kuenen, J. *The Copernicus Atmosphere Monitoring Service Global and Regional Emissions (April 2019 Version)*; Copernicus Atmosphere Monitoring Service (CAMS): Reading, UK, 2019; hal-02322431. [CrossRef]
24. Chevallier, F.; Ciais, P.; Conway, T.J.; Aalto, T.; Anderson, B.E.; Bousquet, P.; Brunke, E.G.; Ciattaglia, L.; Esaki, Y.; Fröhlich, M.; et al. CO_2 surface fluxes at grid point scale estimated from a global 21 year reanalysis of atmospheric measurements. *J. Geophys. Res.* **2010**, *115*, D21307. [CrossRef]
25. Bergamaschi, P.; Houweling, S.; Segers, A.; Krol, M.; Frankenberg, C.; Scheepmaker, R.A.; Dlugokencky, E.; Wofsy, S.C.; Kort, E.A.; Sweeney, C.; et al. Atmospheric CH_4 in the first decade of the 21st century: Inverse modeling analysis using SCIAMACHY satellite retrievals and NOAA surface measurements. *J. Geophys. Res. Atmos.* **2013**, *118*, 7350–7369. [CrossRef]
26. Thompson, R.L.; Chevallier, F.; Crotwell, A.M.; Dutton, G.; Langenfelds, R.L.; Prinn, R.G.; Weiss, R.F.; Tohjima, Y.; Nakazawa, T.; Krummel, P.B.; et al. Nitrous oxide emissions 1999 to 2009 from a global atmospheric inversion. *Atmos. Chem. Phys.* **2014**, *14*, 1801–1817. [CrossRef]
27. Suni, T.; Berninger, F.; Markkanen, T.; Keronen, P.; Rannik, U.; Vesala, T. Interannual variability and timing of growing-season CO_2 exchange in a boreal forest. *J. Geophys. Res. Atmos.* **2003**, *108*, 4265. [CrossRef]
28. Lan, X.; Tans, P.; Thoning, K.W. Trends in Globally-Averaged CO_2 Determined from NOAA Global Monitoring Laboratory Measurements. 2025. Available online: https://gml.noaa.gov/ccgg/trends/global.html?doi=10.15138/9n0h-zh07 (accessed on 11 February 2026). [CrossRef]
29. Kourtidis, K.; Tzivleris, A.; Stathopoulos, S.; Gemitzi, A.; Georgoulias, A.K. On the Methane Emissions of the Greater Thessaloniki Area. *Environ. Sci. Proc.* **2023**, *26*, 39. [CrossRef]
30. Müller, J.; Stavrakou, T.; Bauwens, M.; George, M.; Hurtmans, D.; Coheur, P.; Clerbaux, C.; Sweeney, C. Top-down CO emissions based on IASI observations and hemispheric constraints on OH levels. *Geophys. Res. Lett.* **2018**, *45*, 1621–1629. [CrossRef]
31. Koukouli, M.-E.; Pseftogkas, A.; Karagkiozidis, D.; Mermigkas, M.; Panou, T.; Balis, D.; Bais, A. Extreme wildfires over Northern Greece during Summer 2023—Part B. Adverse effects on regional air quality. *Atmos. Res.* **2025**, *320*, 108034. [CrossRef]
32. Zanis, P.; Hadjinicolaou, P.; Pozzer, A.; Tyrlis, E.; Dafka, S.; Mihalopoulos, N.; Lelieveld, J. Summertime free-tropospheric ozone pool over the eastern Mediterranean/Middle East. *Atmos. Chem. Phys.* **2014**, *14*, 115–132. [CrossRef]
33. Agustí-Panareda, A.; McNorton, J.; Balsamo, G.; Baier, B.C.; Bousserez, N.; Boussetta, S.; Brunner, D.; Chevallier, F.; Choulga, M.; Diamantakis, M.; et al. Global nature run data with realistic high-resolution carbon weather for the year of the Paris Agreement. *Sci. Data* **2022**, *9*, 160. [CrossRef]
34. European Commission; Joint Research Centre; Crippa, M.; Guizzardi, D.; Pagani, F.; Banja, M.; Muntean, M.; Schaaf, E.; Monforti-Ferrario, F.; Becker, W.E.; et al. *GHG Emissions of All World Countries*; Publications Office of the European Union: Luxembourg, 2024; JRC138862. Available online: https://data.europa.eu/doi/10.2760/4002897 (accessed on 11 February 2026).
35. MEEN. *National Inventory Report of Greece for Greenhouse and Other Gases for the Years 1990–2023*; Technical Report; Ministry of Environment and Energy: Athens, Greece, 2021. Available online: https://ypen.gov.gr/wp-content/uploads/2025/04/2025_NIR_Greece.pdf (accessed on 8 April 2026).
36. Zhao, J.; Ciais, P.; Chevallier, F.; Canadell, J.G.; van der Velde, I.R.; Chuvieco, E.; Chen, Y.; Zhang, Q.; He, K.; Zheng, B. Enhanced CH_4 emissions from global wildfires likely due to undetected small fires. *Nat. Commun.* **2025**, *16*, 804. [CrossRef] [PubMed]
37. Xue, C.; Krysztofiak, G.; Ren, Y.; Cai, M.; Mercier, P.; Le Fur, F.; Robin, C.; Grosselin, B.; Daële, V.; McGillen, M.R.; et al. A study on wildfire impacts on greenhouse gas emissions and regional air quality in South of Orléans, France. *J. Environ. Sci.* **2024**, *135*, 521–533. [CrossRef] [PubMed]

38. Strode, S.A.; Duncan, B.N.; Yegorova, E.A.; Kouatchou, J.; Ziemke, J.R.; Douglass, A.R. Implications of carbon monoxide bias for methane lifetime and atmospheric composition in chemistry climate models. *Atmos. Chem. Phys.* **2015**, *15*, 11789–11805. [CrossRef]
39. Chen, W.; Zhang, Y.; Liang, R. Converging evidence for reduced global atmospheric oxidation in 2020. *Natl. Sci. Rev.* **2025**, *12*, nwaf232. [CrossRef] [PubMed]
40. Ciais, P.; Zhu, Y.; Cai, Y.; Lan, X.; Michel, S.E.; Zheng, B.; Zhao, Y.; Hauglustaine, D.A.; Lin, X.; Zhang, Y.; et al. Why methane surged in the atmosphere during the early 2020s. *Science* **2026**, *391*, eadx8262. [CrossRef] [PubMed]
41. European Commission. Climate Action Progress Report 2024: Country profile—Greece. Directorate-General for Climate Action. 2025. Available online: https://climate.ec.europa.eu/eu-action/climate-strategies-targets/progress-climate-action_en (accessed on 11 February 2026).
42. Crippa, M.; Guizzardi, D.; Solazzo, E.; Muntean, M.; Schaaf, E.; Monforti-Ferrario, F.; Vignati, E.; European Commission; Joint Research Centre (JRC). GHG Emissions of All World Countries (EDGAR Database). 2024. Available online: https://edgar.jrc.ec.europa.eu (accessed on 11 February 2026).
43. Germanwatch; NewClimate Institute; Climate Action Network. Climate Change Performance Index 2026: Greece Country Profile. 2026. Available online: https://ccpi.org/country/grc/ (accessed on 11 February 2026).